Unconventional secretion of α-synuclein mediated by palmitoylated DNAJC5 oligomers

Shenjie Wu[1], Daniel W. Sirkis[2], Randy Schekman[1*]

[1]Department of Molecular and Cell Biology, Howard Hughes Medical Institute, University of California, Berkeley, Berkeley, United States; [2]Memory and Aging Center, Department of Neurology, University of California San Francisco, San Francisco, United States

*For correspondence:

schekman@berkeley.edu

Abstract

Alpha-synuclein (α-syn), a major component of Lewy bodies found in Parkinson's disease (PD) patients, has been found exported outside of cells and may mediate its toxicity via cell-to-cell transmission. Here, we reconstituted soluble, monomeric α-syn secretion by the expression of DnaJ homolog subfamily C member 5 (DNAJC5) in HEK293T cells. DNAJC5 undergoes palmitoylation and anchors on the membrane. Palmitoylation is essential for DNAJC5-induced α-syn secretion, and the secretion is not limited by substrate size or unfolding. Cytosolic α-syn is actively translocated and sequestered in an endosomal membrane compartment in a DNAJC5-dependent manner. Reduction of α-syn secretion caused by a palmitoylation-deficient mutation in DNAJC5 can be reversed by a membrane-targeting peptide fusion-induced oligomerization of DNAJC5. We propose that DNAJC5 forms a palmitoylated oligomer to accommodate and export α-syn.

Introduction

Parkinson's disease, the second most common neurodegenerative disease, is characterized by the deposit of clumps of protein aggregate, lipid and damaged organelles known as Lewy bodies (LBs) (Dauer and Przedborski, 2003; Shahmoradian et al., 2019). One of the main constituents of LB is the presynaptic protein α-syn (Stefanis, 2012). α-syn is encoded by the *SNCA* gene and is highly abundant in neurons. As a small, intrinsically disordered protein containing 140 amino acids (AA), α-syn can be divided into three domains, an amphipathic N-terminal domain where most PD-related mutations are located, including A30P, E46K and A53T, a central hydrophobic region known as the non-amyloid-β component (NAC) which is essential for aggregation, and an acidic C-terminal domain (**Fig 1A**) (Alderson and Markley, 2013). α-syn can undergo a conformational change from a disordered monomer to an oligomer (Burre et al., 2014; Lashuel et al., 2002), which can further polymerize to form insoluble fibrils (Guerrero-Ferreira et al., 2019; Guerrero-Ferreira et al., 2018; Strohaker et al., 2019).

In recent years, studies have suggested that α-syn deposits are not static, but rather actively spread during disease progression. Grafted neurons in PD patients developed α-syn positive LBs years after surgery, suggesting host-to-graft pathology propagation (Kordower et al., 2008; Li et al., 2008). Based on analysis of human pathology, the Braak hypothesis posits that α-syn aggregates can spread in a stereotyped manner from the gastrointestinal tract to the brain, causing neuron loss beginning in the brainstem, extending to the midbrain, and finally to the cortex (Braak et al., 2006; Braak et al., 2003).In more recent work, Braak-like transmission of *in vitro* generated α-syn fibrils has been recapitulated in mice and

51 non-human primates (Chu et al., 2019; Chung et al., 2020; Kim et al., 2019; Luk et
52 al., 2012).

53 Less-well understood is the molecular and cellular basis for the transfer of α-syn
54 between cells. Several mechanisms have been proposed for α-syn export and
55 transfer, including unconventional exocytosis (Jang et al., 2010; Lee et al., 2005),
56 exosomes (Danzer et al., 2012; Emmanouilidou et al., 2010; Stykel et al., 2021)
57 and membrane nanotubes (Abounit et al., 2016; Scheiblich et al., 2021). The
58 extracellular existence of α-syn was confirmed in body fluid such as blood and
59 cerebrospinal fluid (CSF) (Borghi et al., 2000; El-Agnaf et al., 2003). Packaging of
60 different conformational forms of α-syn inside extracellular vesicles (EVs) has
61 been reported but requires further vigorous scrutiny to differentiate from secreted
62 sedimentable aggregates (Brahic et al., 2016).

63 DNAJC5, also known as cysteine string protein α (CSPα), is a co-chaperone of
64 HSC70 and has been shown to control the extracellular release of many
65 neurodegenerative disease proteins including α-syn. This process of
66 unconventional traffic has been termed misfolding-associated protein secretion
67 (MAPS) (Fontaine et al., 2016; Lee et al., 2016). DNAJC5 contains three domains
68 – a common N-terminal J-domain conserved among DnaJ proteins, the cysteine-
69 string (CS) central domain which is heavily palmitoylated and anchors the protein
70 to late endosomes, and an overall disordered C-terminal domain (**Fig 1A**).
71 DNAJC5 plays a neuroprotective role in the brain (Zinsmaier, 2010). Depletion of
72 DNAJC5 produces neurodegeneration in mice by cooperation with α-syn (Chandra
73 et al., 2005). Interestingly, a previous study also reported that neuron-derived EVs
74 contain DNAJC5 (Deng et al., 2017). However, the mechanism by which DNAJC5

recognizes and translocates soluble α-syn into a membrane compartment for secretion remains elusive.

In this study, we characterized the mechanism of DNAJC5-induced α-syn secretion in a cell-based secretion assay. Using biochemical characterization and imaging of internalized α-syn in enlarged endosomes as a secretory intermediate, we found previously underappreciated roles of palmitoylation and oligomerization of DNAJC5 in the regulation of α-syn secretion.

Results

Reconstitution of DNAJC5-induced α-syn secretion

Previous studies have shown that α-syn secretion can be stimulated by over-expressing DNAJC5 (Fontaine et al., 2016). The CS domain of DNAJC5 plays a role in promoting stable membrane attachment based on its overall hydrophobicity and by enabling post-translational palmitoylation catalyzed by membrane-bound Asp-His-His-Cys (DHHC) family palmitoyltransferases (Greaves and Chamberlain, 2006). Using a common human cell line, HEK293T, we first tested the expression and subcellular localization of DNAJC5 (**Fig 1B**). Further subcellular enrichment of DNAJC5 was characterized using a C-terminal FLAG tag. Coomassie blue staining revealed two bands of high and low mobility on SDS-PAGE in the membrane and cytosolic fractions, respectively (**Fig 1C**). Similar migration profiles of pamitoylated (P-) and non-palmitoylated (NP-) DNAJC5 have been reported (Greaves et al., 2012). Thus, we confirm that membrane anchoring of DNAJC5 requires palmitoylation in our assay.

98 We next co-expressed DNAJC5 together with α-syn to examine their secretion
99 over time. At 16 h after transfection, we detected similar basal-level secretion of α-
100 syn in both DNAJC5-negative and -positive conditions. Two bands of DNAJC5
101 corresponding to P-DNAJC5 and NP-DNAJC5 were seen in the lysate, but only
102 the P-DNAJC5 was secreted into the medium (**Fig 1D**). The stimulation of α-syn
103 secretion by DNAJC5 became obvious at a longer incubation time (36 h), and at
104 this time point NP-DNAJC5 was also enriched in the medium (**Fig 1E**). In addition
105 to wild-type (WT) α-syn, secretion of several PD-causing α-syn mutant proteins
106 (A30P, E46K and A53T) were also induced by expressing DNAJC5 (**Fig 1**
107 **supplement 1**).

108 In addition to the stimulated secretion of α-syn produced by the expression of
109 exogenous DNAJC5, we examined the dependence of a basal secretion of α-syn on
110 endogenous DNAJC5. We fused α-syn with an N-terminal nanoluciferase (Nluc)
111 (England et al., 2016) for sensitive, quantitative detection (**Fig 1 supplement 2A**).
112 Stimulated secretion of Nluc-α-syn by DNAJC5 was confirmed by immunoblot,
113 indicating that Nluc-fusion did not impede α-syn secretion (**Fig 1 supplement 2B**).
114 Without over-expression of DNAJC5, we observed accumulation of Nluc-α-syn
115 signal in the medium over time (**Fig 1 supplement 2C**). Quercetin is a plant-derived
116 flavonoid that has previously been shown to inhibit DNAJC5-mediated trafficking
117 of a bacterial toxin (**Fig 1 supplement 2D**) (Deruelle et al., 2021). Likewise, we
118 found that quercetin also inhibited Nluc-α-syn secretion in a dose-dependent manner
119 (**Fig 1 supplement 2E**), implying a role for endogenous DNAJC5 in α-syn secretion.
120 Direct depletion of endogenous DNAJC5 by siRNA interference (**Fig 1 supplement**

121 **2F**) also decreased basal α-syn secretion (**Fig 1 supplement 2G**). Taken together,
122 we established a cell-based α-syn secretion assay that is regulated by DNAJC5.

123 **Characterization of extracellular DNAJC5 and α-syn**

124 In our established assay, DNAJC5 and α-syn co-secrete into the medium (**Fig 1E**).
125 Secreted α-syn has been reported to be encapsulated inside EVs (Danzer et al., 2012).
126 We sought to assess the EV association of secreted α-syn using a medium
127 fractionation protocol based on EV preparations developed by our lab (**Fig 2A**)
128 (Shurtleff et al., 2016). After serial differential centrifugation, α-syn and NP-
129 DNAJC5 remained soluble. In comparison, P-DNAJC5 co-sedimented with other
130 EV markers after 100k xg centrifugation (**Fig 2B**). In addition to WT α-syn, we also
131 conducted medium fractionation with several PD-causing α-syn mutants and found
132 they all remained soluble in culture supernatant fractions (**Fig 2 supplement 1A**).
133 To test the EV association of P-DNAJC5, we performed a further sucrose step
134 gradient flotation (**Fig 2 supplement 2A**) with the 100k high-speed pellet fraction
135 (**Fig 2 supplement 2B**). P-DNAJC5 equilibrated with other EV markers to the
136 10%/40% interface expected for buoyant EVs (**Fig 2 supplement 2B**). We conclude
137 that the secreted α-syn induced by DNAJC5 is neither membrane bound nor in an
138 insoluble fibrillar form.

139 Next we sought to characterize the conformation of secreted soluble α-syn. The
140 medium containing secreted α-syn was pooled, concentrated and applied to a gel
141 filtration column. Extracellular α-syn was eluted from the column at around 60%
142 of the column volume (**Fig 2C**), similar to the elution volume of purified monomeric
143 α-syn (**Fig 2D and Fig 2 supplement 3E&F**). By an orthogonal assay, we examined

144 the interaction between tagged and untagged forms of secreted α-syn as an indicator
145 of oligomerization. In this assay, equal amounts of plasmids expressing FLAG-
146 tagged α-syn and non-tagged α-syn were co-transfected in HEK293T cells and the
147 medium was collected and incubated with anti-FLAG M2 beads for to detect co-
148 immunoprecipitation of the two forms (IP) (**Fig 2E**). FLAG-tagged α-syn migrated
149 more slowly that non-tagged α-syn as detected in samples of the culture medium
150 (**Fig 2F**). We found that only the FLAG-tagged α-syn was immuno-precipitated (**Fig**
151 **2F**), suggesting no stable interaction between the two species. The gel filtration and
152 IP assays reinforced our conclusion that α-syn is secreted as a monomer.

153 **Secretion of α-syn requires palmitoylation of DNAJC5**

154 Membrane targeting of DNAJC5 is dependent upon palmitoylation (Greaves et al.,
155 2008). Two specific mutations, L115R and L116Δ in the CS domains, cause adult-
156 onset neuronal ceroid lipofuscinosis (NCL), a type of neurodegenerative disorder
157 (Benitez et al., 2011). NCL mutations reduce the level of DNAJC5 palmitoylation
158 and promote aggregation of the protein (Diez-Ardanuy et al., 2017). We perturbed
159 DNAJC5 palmitoylation by either introducing the palmitoylation-deficient mutation
160 L115R or treating cells with the competitive palmitoyl transferase inhibitor, 2-
161 bromopalmitic acid (2-BA) (Resh, 2006), and subsequently examined the influence
162 on DNAJC5 membrane association. DNAJC5 palmitoylation largely decreased in
163 the L115R mutant or upon 2-BA treatment. Correspondingly, NP-DNAJC5
164 accumulated in the cytosol (**Fig 3A**).

165 Having confirmed palmitoylation inhibition by 2-BA and the L115R mutation, we
166 next examined their effect on α-syn secretion. Upon 10 μM 2-BA treatment, α-syn
167 and DNAJC5 secretion was totally abolished (**Fig 3B**). The efficacy of the inhibitor

168 was validated by the disappearance of the low-mobility band corresponding to P-
169 DNAJC5 in the cell lysate (**Fig 3C**). Furthermore, 2-BA inhibited α-syn secretion in
170 a concentration-dependent manner (**Fig 3 supplement 1B&C**). Likewise, α-syn
171 secretion was reduced by the palmitoylation-deficient DNAJC5 (L115R) compared
172 with DNAJC5 (WT) (**Fig 3D & 3E**). DNAJC5 has been proposed to function
173 downstream of deubiquitinase USP19 in the MAPS pathway (Xu et al., 2018). In
174 agreement with the model, DNAJC5 carrying either NCL mutation L115R or L116Δ
175 had no palmitoylated band detected in the lysate (**Fig 3 supplement 2B**) and blocked
176 USP19-stimulated α-syn secretion (**Fig 3 supplement 2A**). These results establish
177 that palmitoylation is essential for DNAJC5 membrane association and function in
178 stimulating α-syn secretion.

179 **DNAJC5-dependent internalization of α-syn into enlarged endosomes**

180 DNAJC5 has been reported to be associated with late endosomes (Lee et al., 2018).
181 Using immunofluorescence (IF) imaging, we found colocalization between
182 endogenous DNAJC5 and the late-endosomal marker CD63 in certain vesicular
183 structures (**Fig 4 supplement 1A**). To visualize the topological localization of
184 DNAJC5 and α-syn inside or outside endosomes, we turned to a U2OS cell line
185 expressing a fluorescent protein-fused, constitutively active form of Rab5 ($Rab5^{Q79L}$)
186 (Bohdanowicz et al., 2012). As a positive control, CD63 was inside the lumen of
187 enlarged endosomes labeled by mCherry-$Rab5^{Q79L}$ (**Fig 4 supplement 1B**). We
188 labeled DNAJC5 with the self-labeling HaloTag for multiple choices of color in live
189 cell imaging (Los et al., 2008). In the lumen of enlarged endosomes, both diffuse
190 and punctate DNAJC5 were found (**Fig 4A**). Unlike WT DNAJC5, the DNAJC5
191 L115R mutant became disperse in the cytosol, rather than being internalized into

192 enlarged endosomes (**Fig 4 supplement 2A**). In contrast, mNeonGreen (mNG)-
193 fused α-syn showed diffuse localization in both the cytosol and nucleus but was
194 completely excluded from enlarged endosomes in L115R mutant cells (**Fig 4B**).
195 Notably, we observed the entry of α-syn into enlarged endosomes containing
196 internalized DNAJC5, implying the translocation of α-syn into the membrane
197 compartment required DNAJC5 (**Fig 4C**). With no luminal localization inside
198 enlarged endosomes, the DNAJC5 L115R mutants also failed to induce entry of α-
199 syn into the same compartments (**Fig 4 supplement 2B**). Consistent with these
200 imaging results, we applied cell fractionation to separate membranes of DNAJC5-
201 and α-syn-expressing cells (**Fig 4D**). A protease protection assay indicated that α-
202 syn and DNAJC5 were partially resistant to digestion by proteinase K in the absence
203 but not in the presence of Triton X-100 consistent with the conclusion that a fraction
204 of the proteins were sequestered within membrane compartments (**Fig 4E)**. Our
205 visual inspection suggests a membrane translocation role for DNAJC5 prior to α-
206 syn secretion.

207 **Size and unfolding are dispensable for α-syn secretion**

208 In our medium fractionation assay, secreted α-syn in the extracellular space was
209 characterized as a soluble monomer (**Fig 2**). We generated a series of tandem repeats
210 of α-syn to mimic its oligomeric states (**Fig 5A**) (Dong et al., 2018). On SDS-PAGE,
211 a-syn tandem repeats showed a larger apparent size than their predicted molecular
212 weights, possibly caused by their extended conformation as intrinsically disordered
213 proteins (**Fig 2 supplement 2**). We first determined that these α-syn tandem repeats
214 could also be secreted upon expression of DNAJC5 (**Fig 5B**), indicating that

215 DNAJC5 can accommodate α-syn of different sizes. Fractionation of the growth
216 medium showed that secreted tandem repeats were also soluble (**Fig 5 supplement**).

217 In conventional and many unconventional secretion processes, the secreted
218 substrates undergo unfolding prior to translocation through a narrow channel across
219 the hydrophobic membrane barrier (Rapoport et al., 2017). We devised an approach
220 to test the possibility of unfolding by fusion of a hyperstable three-helix bundle (3H)
221 to either the N- or C-terminus of α-syn to impede the unfolding process (**Fig 5D**).
222 This 3H protein was previously designed in the lowest-energy arrangements and
223 displayed extreme thermodynamic stability and remained folded even in non-
224 physiological denaturing conditions (Huang et al., 2014). The α-syn fusion proteins
225 were expressed successfully in cells and co-secreted with DNAJC5 normally into
226 the medium (**Fig 5F**). These data suggest that protein unfolding is dispensable for
227 α-syn secretion.

228 **XPACK fusion rescues DNAJC5 L115R secretion deficiency by induced**
229 **oligomerization**

230 DNAJC5 has been reported to have an intrinsic propensity to form SDS-resistant
231 oligomers (Zhang and Chandra, 2014). In the whole membrane immunoblot of
232 extracellular DNAJC5, we noticed many diffuse, ladder-like bands above the two
233 corresponding to P-DNAJC5 and NP-DNAJC5 (**Fig 6A**), possibly higher molecular
234 weight (HMW) oligomers. This apparent oligomerization of DNAJC5 became more
235 obvious when the J domain was deleted (**Fig 6 supplement 1A**). The formation of
236 HMW-DNAJC5 was not due to inter-molecular disulfide bonds because the diffuse
237 bands persisted in the presence of a reducing agent (**Fig 6 supplement 1B**). To assess
238 the size of these HMW species of DNAJC5, we evaluated a cell lysate by gel

239 filtration chromatography. HMW-DNAJC5 fractionated according to its apparent
240 size, forming a stair-like pattern on the DNAJC5 immunoblot (**Fig 6B**). HMW-
241 DNAJC5 appeared not to be in protein aggregates based chromatography within the
242 gel filtration column volume (**Fig 6B**). These results suggest the presence of higher-
243 ordered, SDS-resistant DNAJC5 oligomers both in intracellular and extracellular
244 fractions.

245 XPACK (XP) is a membrane-targeting peptide sequence used widely in studies of
246 cargo loading into exosomes and delivery to target cells of choice (Yim et al., 2016).
247 The exosome loading process by XPACK is also dependent on two lipidation
248 reactions – myristoylation on the first glycine and palmitoylation on the second
249 cysteine (**Fig 6 supplement 1C**) (Zacharias et al., 2002). Given the similarity of
250 membrane localization and lipidation between XPACK and the CS domain of
251 DNAJC5, we tested the effect of XPACK fusion with DNAJC5 on the latter's ability
252 to induce α-syn secretion. Upon fusion with XPACK to the N-terminus, only one
253 band with same mobility as P-DNAJC5 appeared in the WT DNAJC5 XPACK
254 fusion protein (XP-WT) sample, in contrast to the two bands of both P- and NP-
255 DNAJC5 in the WT DNAJC5 sample (**Fig 6 supplement 1D**). Furthermore, XP-
256 DNAJC5 was tightly associated with membranes (**Fig 6 supplement 1E**). This
257 suggested that XPACK lipidation is non-reversible, resulting in complete lipidation
258 of DNAJC5. Both the slow electrophoretic mobility and membrane association of
259 XP-DNAJC5 were reversed by 2-BA treatment, indicating XPACK lipidation
260 included palmitoylation (**Fig 6 supplement 1E**). We also examined the effect of
261 XPACK fusion on the palmitoylation-deficient mutant of DNAJC5 (L115R). In this
262 case, XPACK fusion did not change the mobility of DNAJC5 mutant L115R from
263 NP-DNAJC5 to P-DNAJC5 but resulted in several weak protein bands between the

264 two (**Fig 6 supplement 1D**). We introduced a point mutation of serine to leucine
265 into the XPACK sequence to block its normal lipidation, naming it Dead XPACK
266 (DXP) (**Fig 6 supplement 1C**). The DXP-DNAJC5 L115R species had the same
267 mobility as NP-DNAJC5 (**Fig 6 supplement 1D**).

268 We conducted the same cellular fractionation with cells expressing DNAJC5 XP-
269 L115R. In this case, XP-L115R migrated slowly and remained near the top of the
270 gels, suggesting XPACK induces high-order oligomerization or aggregation of
271 DNAJC5 L115R (**Fig 6C**). XP-L115R was also highly enriched in the membrane
272 fraction through XPACK-mediated lipidation (**Fig 6C**). In spite of this apparent
273 difference between DNAJC5 XP-L115R and WT DNAJC5, α-syn secretion was
274 stimulated by the expression of both species (**Fig 6D**). Treatment with the
275 palmitoylation inhibitor 2-BA restored mobility of XP-L115R to a position similar
276 to that of monomeric DNAJC5 (**Fig 6E**). Correspondingly, secretion of α-syn was
277 no longer stimulated by the palmitoylation deficient DNAJC5 XP-L115R monomer
278 (**Fig 6D**).

279 The data from the cellular fractionation and secretion assays showed similar effects
280 for WT DNAJC5 and DNAJC5 XP-L115R. We employed imaging methods to
281 examine the subcellular localization of DNAJC5 XP-L115R fused with a C-terminal
282 HaloTag. In contrast to the diffuse distribution of the DNAJC5 L115R mutant, which
283 was excluded from the interior of enlarged endosomes (**Fig 4 supplement 2A**),
284 punctate DNAJC5 XP-L115R were widely associated with enlarged endosomes (**Fig
285 6 supplement 2A**). Internalization events were found in several enlarged endosomes
286 (**Fig 6 supplement 2A, magnified insets**). mNG-α-syn was also incorporated into
287 endosomal compartments when co-expressed with DNAJC5 XP-L115R (**Fig 6**

288 **supplement 2B**). Our imaging data corroborate the biochemical similarity between
289 WT DNAJC5 and DNAJC5 XP-L115R.

290 **The J domain and C-terminal tail (C tail) of DNAJC5 are dispensable for α-syn**
291 **secretion**

292 The secretion deficiency caused by the L115R mutation highlights the importance
293 of the CS domain of DNAJC5 in regulating α-syn secretion. The structure of the J
294 domain of DNAJC5 has been solved by nuclear magnetic resonance (NMR) (Patel
295 et al., 2016). Recent progress in deep learning algorithms, exemplified by AlphaFold,
296 enables atomic accuracy in protein structure prediction (Jumper et al., 2021). We
297 searched the public AlphaFold database to examine the predicted structure of full-
298 length DNAJC5. In the predicted structure, the J domain shows a conserved overall
299 globular J protein fold on the N-terminus, linked by the helical CS domain to the
300 flexible C-terminal tail. Only a short helix is predicted to reside within the C-tail
301 (**Fig 7A**). We refined the boundary of each domain in DNAJC5 based on the
302 predicted structure.

303 Using this information, we showed that oligomerization of DNAJC5 increased when
304 the J domain was deleted (**Fig 6 supplement 1A and Fig 7C**). Deletion of the J
305 domain did not alter the level of α-syn secretion induced by DNAJC5, indicating
306 that this domain was dispensable for α-syn secretion (**Fig 7B**). Next, we examined
307 the function of the C-tail by truncating about ten amino acids at a time, resulting in
308 a series of C-terminal truncated DNAJC5 constructs, i.e., DNAJC5 ΔC10, ΔC20,
309 ΔC30, ΔC40. All four DNAJC5 C-terminal truncations were able expressed and
310 formed oligomers in cells (**Fig 7E**). C-terminal truncated oligomers were co-secreted

311 with α-syn into the medium (**Fig 7D**). This result demonstrates that neither the J
312 domain nor the C-tail is required for DNAJC5 to induce α-syn secretion.

313

314 Discussion

315 Transmission of protein aggregates and subsequent self-amplification is emerging
316 as a common theme across various neurodegenerative diseases. DNAJC5 has been
317 shown to control the release of neurodegenerative disease proteins but the detailed
318 molecular mechanism remains elusive. In this study, we first reconstituted
319 DNAJC5-regulated α-syn secretion in cultured HEK293T cells. By combining this
320 assay with medium and cellular fractionation, we demonstrated that membrane-
321 anchoring of DNAJC5 through palmitoylation is crucial for its secretion and the
322 secreted α-syn as a soluble monomer. In addition, we observed the topological
323 locations of DNAJC5 and α-syn inside enlarged endosomes, presumably at an
324 intermediate stage prior to secretion. Furthermore, artificially-devised lipidation
325 (XPACK) induced DNAJC5 oligomers and restored α-syn secretion. Finally, we
326 provide evidence that both palmitoylation and oligomerization are solely
327 dependent on the CS domain, which is required for α-syn secretion. Based on our
328 biochemical assays and imaging observations, we propose that palmitoylated
329 DNAJC5 oligomers function at a step involving membrane translocation of
330 cytosolic α-syn, enabling it to become competent for secretion (**Fig 7F**).

331 Using the criteria of differential sedimentation and gel filtration chromatography,
332 we conclude that α-syn is secreted in cultures cells as a soluble monomeric species
333 not enclosed within extracellular vesicles, regardless of mutations modeled on PD
334 (**Fig 2 supplement 1A**) or as expressed in tandem arrays or in gene fusions to

335 tightly folded proteins (**Fig 5 supplement**). Consistent with our results, other
336 MAPS substrates were also reported to be soluble (Lee et al., 2016). Although α-
337 syn oligomers have also been found in EVs (Danzer et al., 2012; Emmanouilidou
338 et al., 2010; Guo et al., 2020) we see no evidence for this in our immunoblot
339 experiments (**Fig 2B**). With a more sensitive and quantitative Nluc assay, 85% of
340 secreted α-syn was found to be soluble (**Fig 2 supplement 1B**). Given that
341 DNAJC5 can be found in membrane buoyant EVs (**Fig 2 supplement 2B**) and α-
342 syn is known to destabilize lipid membrane (Fusco et al., 2017), we sought to
343 detect soluble EV luminal proteins as an indicator that a-syn may have escaped by
344 rupture of the EV membrane. However, we failed to see any increase in EV
345 luminal markers in the high-speed supernatant fraction from cells overexpressing
346 α-syn (**data not shown**). How α-syn passes across a membrane *en route* to
347 secretion and whether insoluble α-syn aggregates can be secreted through the same
348 pathway, remain to be addressed.

349 Numerous neuronal proteins are palmitoylated, including synaptic scaffolding
350 proteins, signaling proteins and synaptic vesicle proteins (Linder and Deschenes,
351 2007). Protein palmitoylation has been implicated in the pathogenesis of
352 neurodegenerative diseases (Cho and Park, 2016). In PD particularly, a recent
353 study reported that upregulation of cellular palmitoylation decreased α-syn
354 cytoplasmic inclusions (Ho et al., 2021). The neuropathology and behavior
355 deficiency of Huntington disease (HD) mice can be reversed by boosting brain
356 palmitoylation (Virlogeux et al., 2021). In the case of DNAJC5, L115R and
357 L116Δ, the two adjacent mutations causing decreased palmitoylation of DNAJC5
358 monomers, lead to a familial form of NCL (Benitez et al., 2011; Diez-Ardanuy et
359 al., 2017). Our results suggested that the secretion of neurodegenerative disease

360 proteins is also dependent on palmitoylation, possibly alleviating the cellular
361 burden of protein aggregate accumulation. Notably, the general inhibition of
362 cellular palmitoylation by 2-BA led to a complete block of α-syn secretion,
363 whereas the specific palmitoylation deficient DNAJC5 mutant L115R only
364 partially decreased α-syn secretion (**Fig 3B-E**). The difference implies the
365 existence of palmitoylation-dependent factors other than DNAJC5.

366 Although DNAJC5 co-expressed with α-syn and palmitoylation are required for
367 secretion, EV-associated P-DNAJC5 clearly separated from soluble α-syn in the
368 culture medium (**Fig 2B and Fig 2 supplement 2B**). At which step do the two
369 separate? In our live cell imaging experiments, the internalized DNAJC5 inside
370 enlarged endosomes had both punctate and diffuse distributions (**Fig 4A**). This
371 may represent the soluble NP-DNAJC5 and membrane-attached P-DNAJC5,
372 respectively. In the time-lapse imaging of internalized α-syn induced by DNAJC5,
373 both DNAJC5 and α-syn moved dynamically inside the compartment, without
374 significant co-localization (**Fig4 supplementary video**). This observation suggests
375 that the separation of DNAJC5 and α-syn may occur prior to their secretion when
376 the late endosome and plasma membrane fuse.

377 Zhang et al. (2020) have reported a novel membrane channel, TMED10, for the
378 unconventional secretion of IL-1β. These authors speculate an activation-on-
379 demand oligomerization of TMED10 membrane subunits to form a conducting
380 channel for substrate translocation, a process they refer to as THU (Zhang et al.,
381 2020). α-syn was reported to not depend on TMED10 for unconventional secretion
382 (Zhang et al., 2020). Similarly, in chaperone-mediated autophagy (CMA),
383 cytosolic substrates are proposed to be translocated into lysosomes through a

384 channel formed by the oligomerization of a single-transmembrane protein,
385 LAMP2A (Bandyopadhyay et al., 2008). The secretion of α-syn has been shown to
386 be independent of CMA (Lee et al., 2018). Without a transmembrane domain,
387 membrane-tethered P-DNAJC5 oligomer is unlikely to be a channel for
388 translocation. A recent preprint has identified CD98hc, an amino acid transporter
389 subunit, to be a DNAJC5 interactor that is required for α-syn secretion (Lee et al.,
390 2021 preprint). It remains to be determined whether CD98hc or other as yet
391 uncharacterized membrane proteins are directly involved in α-syn membrane
392 translocation.

393 In SEC61-mediated co-translational translocation, substrates enter the SEC61
394 translocon in an unfolded state (Rapoport et al., 2017). In THU and CMA,
395 substrate unfolding is also required for translocation across the membrane
396 (Kaushik and Cuervo, 2018; Zhang et al., 2020). In striking contrast, unfolding and
397 size is not a limiting factor for α-syn secretion (**Fig 5**). As a precedent of
398 translocation without unfolding, studies have shown the import of folded proteins
399 into the matrix of peroxisomes and obviously through the nuclear pore (Kim and
400 Hettema, 2015; Lin and Hoelz, 2019). DNAJC5 forms a series of extremely stable
401 oligomers, which may provide versatile adaptors to accommodate diverse
402 misfolded or folded substrates with different dimensions. The structure of
403 DNAJC5 oligomers may shed light on the principle of this folding-independent
404 translocation pathway.

405

406 **Materials and methods**

407

408 **Key Resources table**

REAGENT or RESOURCE	SOURCE	IDENTIFIER
Antibodies		
Mouse monoclonal anti-α-synuclein	BD Biosciences	Cat# 610787
Rabbit polyclonal anti-DNAJC5	RayBiotech	Cat# 144-10489-200
Mouse monoclonal anti-alpha Tubulin	Abcam	Cat# ab7291
Mouse monoclonal anti-Alix	Santa Cruz Biotechnology	Cat# Sc-53540
Rabbit monoclonal anti-CD9	Cell Signaling Technology	Cat# 13174S
Mouse monoclonal anti-PDI	Enzo Life Sciences	Cat# ADI-SPA-891-D
Mouse monoclonal anti-CD63	Fisher Scientific	Cat# BDB556019
Mouse monoclonal anti-Flotillin-2	BD Biosciences	Cat# 610383
Mouse monoclonal anti-Transferrin Receptor	Thermo Fisher SCIENTIFIC	Cat# 13-6800
Mouse monoclonal anti-FLAG	Sigma-Aldrich	Cat# F9291
Bacterial and virus strains		
XL1-Blue competent cells	MacroLab Berkeley	N/A
Rossetta (DE3) pLysS competent cells	MacroLab Berkeley	N/A
Chemicals, peptides, and recombinant proteins		
Anti-FLAG M2 Affinity Gel	Sigma-Aldrich	Cat# A2220-5ML
Dimethyl sulfoxide (DMSO)	Fisher Scientific	Cat# BP231-100
Quercetin	Sigma-Aldrich	Cat# Q4951-10G

2-Bromopalmitic acid	Millipore Sigma	Cat# 21604-1G
HaloTag® Oregon Green® Ligand	Promega	Cat# G2802
HaloTag® TMR® Ligand	Promega	Cat# G8251
Prolong Gold with DAPI	Fisher Scientific	Cat# P36931
α-syn tandem repeats protein	This paper	N/A
Critical Commercial Assays		
Nano-Glo® Luciferase Assay System	Promega	Cat# N1150
Experimental Models: Cell Lines		
HEK293T Cells	Cell culture facility, UC Berkeley	N/A
U2OS Cells	Cell culture facility, UC Berkeley	N/A
Oliogonucleotides		
FlexiTube GeneSolution GS80331for DNAJC5	Qiagen	1027416
Recombinant DNA plasmids		
mCherry-Rab5CA(Q79L)	Addgene	Cat# 35138
BFP-Rab5CA(Q79L)	This study	N/A
SNCA (Myc-DDK-tagged)-Human synuclein, apha	OriGene Technoogy	Cat# RC221446
CSP (DNAJC5) (NM_025219) Human Tagged ORF Clone	OriGene Technology	Cat# RC208826
TCH1003-MGC premier cDNA clone for USP19	transOMIC	Cat# TCH1003

α-synuclein-A30P	Gift of Dr. Thomas Südhof lab	N/A
α-synuclein-E46K	Gift of Dr. Thomas Südhof lab	N/A
α-synuclein-A53T	Gift of Dr. Thomas Südhof lab	N/A
αS-2 (α-syn-α-syn) tandem dimer	Gift of Michael Woodside lab	N/A
αS-4 (α-syn-α-syn-α-syn-α-syn) tandem Tetramer	Gift of Michael Woodside lab	N/A
DNAJC5-L115R	This study	N/A
DNAJC5-L116Δ	This study	N/A
DNAJC5 (WT)-HaloTag	This study	N/A
DNAJC5 (L115R)-HaloTag	This study	N/A
XPACK-DNAJC5 (L115R)-HaloTag	This study	N/A
mNeonGreen-α-synuclein	This study	N/A
3H-α-synuclein	This study	N/A
α-synuclein-3H	This study	N/A
XPACK-DNAJC5 (WT)	This study	N/A
XPACK-DNAJC5 (L115R)	This study	N/A
DEAD XPACK-DNAJC5 (L115R)	This study	N/A
DNAJC5-ΔJ (Δ14-82)	This study	N/A
DNAJC5-ΔC10 (D189-198)	This study	N/A

DNAJC5-ΔC20 (D179-198)	This study	N/A
DNAJC5-ΔC30 (D169-198)	This study	N/A
DNAJC5-ΔC40 (D151-198)	This study	N/A
Software and algorithms		
Fiji (ImageJ)	NIH	https://imagej.nih.gov/ij/
PyMOL	Schrödinger	https//pymol.org/2/
Prism 8	Graphpad	https://www.graphpad.com/scientific-software/prism/
AlphaFold Protein Structure Database	DeepMind	https://alphafold.ebi.ac.uk/

409

410 **Cell culture and transfection**

411 Cells were grown at 37°C in 5% CO2 and maintained in Dulbecco's modified
412 Eagle's medium (DMEM) supplemented with 10% fetal bovine serum (FBS). For
413 secretion assays, the FBS concentration was reduced to 1% for up to 36 h. The
414 growth rate of cells slowed down but the cells remained viable. For EV preparation
415 and medium fractionation, cells were grown in DMEM supplemented with
416 exosome-depleted FBS. Exosome-depleted FBS was prepared by overnight
417 centrifugation of 30% diluted FBS in DMEM at 100,000xg. Transfection of
418 plasmids into cells was performed using Lipofectamine 2000 (Thermo Fisher
419 Scientific, Waltham, MA) according to the manufacturer's protocols. SiRNA
420 knockdown was performed using Lipofectamine RNAiMAX reagent (Thermo
421 Fisher Scientific, Waltham, MA) according to the manufacturer's protocols.

422 **Reconstitution of α-syn secretion in HEK293T cells**

423 HEK293T cells (cultured in 6-well plates) were cultured to 60% confluence and
424 co-transfected with plasmids encoding different constructs of α-syn and DNAJC5.

425 At 4 h after transfection, cell culture medium was replaced with DMEM
426 supplemented with 1% FBS containing indicated drugs for treatment. At indicated
427 time points, media fractions were collected and centrifuged at 1,000xg for 10 min
428 to remove floating cells and cell debris. The media were mixed with
429 methanol/chloroform to precipitate proteins which were collected by centrifugation
430 (10,000 g x 10 min) and resuspended in SDS-PAGE sample loading buffer to
431 achieve concentration (20-fold). Cells were lysed in lysis buffer (10 mM Tris, pH
432 7.4, 100 mM NaCl, 1% Triton X-100). Both the concentrated media and cell lysate
433 fractions were analyzed by immunoblot.

434 For a nanoluciferase-based assay, the media fractions were collected and
435 centrifuged at 1,000xg for 10 min. The supernatant fractions were harvested and
436 further diluted with PBS buffer (1000-fold). The nanoluciferase activity was
437 assayed using a Nano-Glo® Luciferase Assay System (Promega, Madison, WI)
438 according to the manufacturer's protocol.

439 **Membrane and Cytosol fractionation**

440 Cells (one 10cm dish) were cultured to 70% confluence and transfected with
441 different constructs of DNAJC5. One day after transfection, the transfected cells
442 were harvested by scraping in 1 ml B88 (20 mM HEPES-KOH, pH 7.2, 250 mM
443 sorbitol, 150 mM potassium acetate and 5 mM magnesium acetate) plus a cocktail
444 of protease inhibitors (Sigma-Aldrich, St. Louis, MO) and were further
445 homogenized by passing through a 22G needle 10 times. Cell homogenates were
446 centrifuged at 500xg for 10 min. The recovered supernatant fractions, post-nuclear
447 supernatant (PNS), were centrifuged at 100,000xg for 1.5 h. The supernatant was
448 collected and the centrifugation was repeated to achieve a clarified cytosol
449 fraction. The pellet fraction was washed and resuspended in the same volume of

450 B88. The resuspended material was also centrifuged again to collect the washed
451 membrane. Membranes were lysed in lysis buffer.

452 For membrane fractionation, the PNS was subjected to differential centrifugation at
453 3,000xg (10 min), 25,000xg (20 min) and 100,000xg (30min). Membrane fractions
454 were normalized to phosphatidylcholine content and analyzed by immunoblot (Ge
455 et al., 2013).

456 For proteinase K protection assays, the 25,000xg membrane fraction was aliquoted
457 into three tubes: one without proteinase K, one with proteinase K (10 μg/ml), and
458 one with proteinase K plus TritonX-100 (0.5%). The reaction was conducted on ice
459 for 20 min and stopped by sequential addition of PMSF (1mM) and sample buffer,
460 which were then heated on metal block at 95°C for 5 min and samples were
461 analyzed by SDS-PAGE and immunoblot.

462 **Medium fractionation and extracellular vesicle preparation**

463 Conditioned medium was harvested and centrifuged first at 1,500xg for 20 min
464 followed by 10,000xg for 30 min and 100,000xg for 1.5 h. The supernatant
465 fractions at each step were collected and treated with methanol/chloroform to
466 precipitate proteins which were then collected by centrifugation and pellet
467 fractions were and resuspended in sample buffer for concentration (20-fold). The
468 sedimented fractions at each step were also collected and resuspended in sample
469 buffer. All the fractions were analyzed by immunoblot.

470 EVs were further floated by a sucrose step gradient centrifugation. The pellet
471 fraction from a 100,000xg centrifugation was resuspended in PBS and mixed with
472 60% sucrose buffer (10mM Tris-HCl pH 7.4, 100 mM NaCl) to achieve a final
473 sucrose concentration >50% as measured with a refractometer. Aliquots of 40% (5

474 ml) and 10% (2 ml) sucrose buffer were sequentially overlaid above the sample.
475 The tubes were then centrifuged at 150,000xg for 16 h in an SW41 Ti swinging-
476 bucket rotor (Beckman Coulter). After centrifugation, fractions (0.5 ml for each)
477 were collected from top to bottom and samples analyzed by SDS PAGE and
478 immunoblot.

479 **Co-immunoprecipitation**

480 Media fractions were collected and centrifuged at 1,000xg for 10min. The
481 supernatant fractions were collected and concentrated (20-fold) using a 10 kDa
482 Amicon filter (Millipore, Billerica, MA). Concentrated media (1 ml) were
483 incubated with 20 μl of anti-FLAG M2 affinity gel (Sigma-Aldrich, St. Louis,
484 MO) for 1 h at 4°C. After washing 5x with lysis buffer, SDS-PAGE sample
485 loading buffer was added to the beads and samples were processed for SDS PAGE
486 and immunoblot.

487 **Protein purification**

488 The purification of different α-syn tandem-oligomer constructs was performed as
489 previously described (Dong et al., 2018). Briefly, an osmotic shock protocol was
490 adapted to enrich proteins released from the periplasm of transfected *E. coli*. The
491 supernatant fraction containing released proteins was subjected to ammonium
492 sulfate (AS) precipitation, with 50%, 45% and 40% saturated concentration of AS
493 for monomer, dimer and tetramer, respectively. After overnight precipitation, the
494 precipitated proteins were collected by centrifugation at 100,000xg for 30 min. The
495 pellet fractions were dissolved in Buffer A (20mM Tris-HCl pH 8.0) and clarified
496 by repeated centrifugation at 100,000xg for 30 min.

497 Clarified supernatants were applied to an equilibrated HiPrep Q Fast Flow 16/10
498 column (GE Healthcare, Chicago, IL). Eluted proteins were collected, concentrated
499 by 10 kDa Amicon filter (Millipore, Billerica, MA) and further purified by gel
500 filtration (Superdex-200, GE Healthcare). PBS was used as gel filtration buffer.
501 Purified proteins were assessed by SDS-PAGE followed by coomassie-blue
502 staining.

503 **Immunofluorescence and live-cell Imaging**

504 For immunofluorescence, U2OS cells were washed once with PBS and
505 immediately fixed by 4% EM-grade paraformaldehyde (Electron Microscopy
506 Science, Hatfield, PA) for 10 min at room temperature. Cells were washed three
507 times with PBS and blocked and permeabilized for 30 min in permeabilization
508 buffer (5% FBS and 0.1% saponin in PBS). Cells were then incubated with 1:100
509 dilution of primary antibodies overnight at 4°C. After three washes with PBS, cells
510 were incubated with 1:500 dilution of fluorophore-conjugated secondary
511 antibodies for 30 min at room temperature. Prolong Gold with DAPI (Thermo
512 Fisher) was used as mounting solution. Images were acquired with a Zeiss
513 LSM900 confocal microscope and analyzed with Fiji/ImageJ software
514 (https://imagej.nih.gov/ij/).

515 For live-cell imaging, cells were cultured in 35mm glass bottom dishes (MatTek).
516 The addition of HaloTag fluorescent ligands were added according to the
517 manufacturer's protocol (Promega). After incubation, the medium was replaced
518 with Opti-MEM supplemented with 10% FBS. Imaging was performed using a
519 Zeiss LSM900 confocal microscope in a temperature-controlled (37°C and 5%
520 CO2) environment.

Additional information

Competing Interests

Randy Schekman: Reviewing Editor and Founding Editor-in-Chief, *eLife*. The other authors declare that no competing interests exist.

Funding

Funder	Grant reference number	Author
Howard Hughes Medical Institute	Investigator	Randy Schekman

The funders had no role in study design, data collection and interpretation, or the decision to submit the work for publication.

Author Contributions

SW, Conception and design, Acquisition of data, Analysis and interpretation of data, Drafting or revising the article; DS, Conception and design, Acquisition of data, Analysis and interpretation of data, Drafting or revising the article; RS, Conception and design, Analysis and interpretation of data, Drafting or revising the article.

References

Abounit, S., Bousset, L., Loria, F., Zhu, S., de Chaumont, F., Pieri, L., Olivo-Marin, J.C., Melki, R., and Zurzolo, C. (2016). Tunneling nanotubes spread fibrillar alpha-synuclein by intercellular trafficking of lysosomes. EMBO J *35*, 2120-2138.

543
544 Alderson, T.R., and Markley, J.L. (2013). Biophysical characterization of alpha-
545 synuclein and its controversial structure. Intrinsically Disord Proteins *1*, 18-39.
546 Bandyopadhyay, U., Kaushik, S., Varticovski, L., and Cuervo, A.M. (2008). The
547 chaperone-mediated autophagy receptor organizes in dynamic protein complexes
548 at the lysosomal membrane. Mol Cell Biol *28*, 5747-5763.
549
550 Benitez, B.A., Alvarado, D., Cai, Y., Mayo, K., Chakraverty, S., Norton, J.,
551 Morris, J.C., Sands, M.S., Goate, A., and Cruchaga, C. (2011). Exome-sequencing
552 confirms DNAJC5 mutations as cause of adult neuronal ceroid-lipofuscinosis.
553 PLoS One *6*, e26741.
554
555 Bohdanowicz, M., Balkin, D.M., De Camilli, P., and Grinstein, S. (2012).
556 Recruitment of OCRL and Inpp5B to phagosomes by Rab5 and APPL1 depletes
557 phosphoinositides and attenuates Akt signaling. Mol Biol Cell *23*, 176-187.
558
559 Borghi, R., Marchese, R., Negro, A., Marinelli, L., Forloni, G., Zaccheo, D.,
560 Abbruzzese, G., and Tabaton, M. (2000). Full length alpha-synuclein is present in
561 cerebrospinal fluid from Parkinson's disease and normal subjects. Neurosci Lett
562 *287*, 65-67.
563
564 Braak, H., de Vos, R.A., Bohl, J., and Del Tredici, K. (2006). Gastric alpha-
565 synuclein immunoreactive inclusions in Meissner's and Auerbach's plexuses in
566 cases staged for Parkinson's disease-related brain pathology. Neurosci Lett *396*,
567 67-72.
568
569 Braak, H., Del Tredici, K., Rub, U., de Vos, R.A., Jansen Steur, E.N., and Braak,
570 E. (2003). Staging of brain pathology related to sporadic Parkinson's disease.
571 Neurobiol Aging *24*, 197-211.
572
573 Brahic, M., Bousset, L., Bieri, G., Melki, R., and Gitler, A.D. (2016). Axonal
574 transport and secretion of fibrillar forms of alpha-synuclein, Abeta42 peptide and
575 HTTExon 1. Acta Neuropathol *131*, 539-548.
576
577 Burre, J., Sharma, M., and Sudhof, T.C. (2014). alpha-Synuclein assembles into
578 higher-order multimers upon membrane binding to promote SNARE complex
579 formation. Proc Natl Acad Sci U S A *111*, E4274-4283.
580

581 Chandra, S., Gallardo, G., Fernandez-Chacon, R., Schluter, O.M., and Sudhof,
582 T.C. (2005). Alpha-synuclein cooperates with CSPalpha in preventing
583 neurodegeneration. Cell *123*, 383-396.
584
585 Cho, E., and Park, M. (2016). Palmitoylation in Alzheimer's disease and other
586 neurodegenerative diseases. Pharmacol Res *111*, 133-151.
587
588 Chu, Y., Muller, S., Tavares, A., Barret, O., Alagille, D., Seibyl, J., Tamagnan, G.,
589 Marek, K., Luk, K.C., Trojanowski, J.Q., *et al*. (2019). Intrastriatal alpha-synuclein
590 fibrils in monkeys: spreading, imaging and neuropathological changes. Brain *142*,
591 3565-3579.
592
593 Chung, H.K., Ho, H.A., Perez-Acuna, D., and Lee, S.J. (2020). Modeling alpha-
594 Synuclein Propagation with Preformed Fibril Injections. J Mov Disord *13*, 77-79.
595
596 Danzer, K.M., Kranich, L.R., Ruf, W.P., Cagsal-Getkin, O., Winslow, A.R., Zhu,
597 L., Vanderburg, C.R., and McLean, P.J. (2012). Exosomal cell-to-cell transmission
598 of alpha synuclein oligomers. Mol Neurodegener *7*, 42.
599
600 Dauer, W., and Przedborski, S. (2003). Parkinson's disease: mechanisms and
601 models. Neuron *39*, 889-909.
602
603 Deng, J., Koutras, C., Donnelier, J., Alshehri, M., Fotouhi, M., Girard, M., Casha,
604 S., McPherson, P.S., Robbins, S.M., and Braun, J.E.A. (2017). Neurons Export
605 Extracellular Vesicles Enriched in Cysteine String Protein and Misfolded Protein
606 Cargo. Sci Rep *7*, 956.
607
608 Deruelle, V., Bouillot, S., Job, V., Taillebourg, E., Fauvarque, M.O., Attree, I., and
609 Huber, P. (2021). The bacterial toxin ExoU requires a host trafficking chaperone
610 for transportation and to induce necrosis. Nat Commun *12*, 4024.
611
612 Diez-Ardanuy, C., Greaves, J., Munro, K.R., Tomkinson, N.C., and Chamberlain,
613 L.H. (2017). A cluster of palmitoylated cysteines are essential for aggregation of
614 cysteine-string protein mutants that cause neuronal ceroid lipofuscinosis. Sci Rep
615 *7*, 10.
616

617 Dong, C., Hoffmann, M., Li, X., Wang, M., Garen, C.R., Petersen, N.O., and
618 Woodside, M.T. (2018). Structural characteristics and membrane interactions of
619 tandem alpha-synuclein oligomers. Sci Rep *8*, 6755.
620
621 El-Agnaf, O.M., Salem, S.A., Paleologou, K.E., Cooper, L.J., Fullwood, N.J.,
622 Gibson, M.J., Curran, M.D., Court, J.A., Mann, D.M., Ikeda, S., *et al*. (2003).
623 Alpha-synuclein implicated in Parkinson's disease is present in extracellular
624 biological fluids, including human plasma. FASEB J *17*, 1945-1947.
625
626 Emmanouilidou, E., Melachroinou, K., Roumeliotis, T., Garbis, S.D., Ntzouni, M.,
627 Margaritis, L.H., Stefanis, L., and Vekrellis, K. (2010). Cell-produced alpha-
628 synuclein is secreted in a calcium-dependent manner by exosomes and impacts
629 neuronal survival. J Neurosci *30*, 6838-6851.
630
631 England, C.G., Ehlerding, E.B., and Cai, W. (2016). NanoLuc: A Small Luciferase
632 Is Brightening Up the Field of Bioluminescence. Bioconjug Chem *27*, 1175-1187.
633
634 Fontaine, S.N., Zheng, D., Sabbagh, J.J., Martin, M.D., Chaput, D., Darling, A.,
635 Trotter, J.H., Stothert, A.R., Nordhues, B.A., Lussier, A., *et al*. (2016).
636 DnaJ/Hsc70 chaperone complexes control the extracellular release of
637 neurodegenerative-associated proteins. EMBO J *35*, 1537-1549.
638
639 Fusco, G., Chen, S.W., Williamson, P.T.F., Cascella, R., Perni, M., Jarvis, J.A.,
640 Cecchi, C., Vendruscolo, M., Chiti, F., Cremades, N., *et al*. (2017). Structural basis
641 of membrane disruption and cellular toxicity by alpha-synuclein oligomers.
642 Science *358*, 1440-1443.
643
644 Ge, L., Melville, D., Zhang, M., and Schekman, R. (2013). The ER-Golgi
645 intermediate compartment is a key membrane source for the LC3 lipidation step of
646 autophagosome biogenesis. Elife *2*, e00947.
647
648 Greaves, J., and Chamberlain, L.H. (2006). Dual role of the cysteine-string domain
649 in membrane binding and palmitoylation-dependent sorting of the molecular
650 chaperone cysteine-string protein. Mol Biol Cell *17*, 4748-4759.
651
652 Greaves, J., Lemonidis, K., Gorleku, O.A., Cruchaga, C., Grefen, C., and
653 Chamberlain, L.H. (2012). Palmitoylation-induced aggregation of cysteine-string

654 protein mutants that cause neuronal ceroid lipofuscinosis. J Biol Chem *287*, 37330-
655 37339.
656
657 Greaves, J., Salaun, C., Fukata, Y., Fukata, M., and Chamberlain, L.H. (2008).
658 Palmitoylation and membrane interactions of the neuroprotective chaperone
659 cysteine-string protein. J Biol Chem *283*, 25014-25026.
660
661 Guerrero-Ferreira, R., Taylor, N.M., Arteni, A.A., Kumari, P., Mona, D., Ringler,
662 P., Britschgi, M., Lauer, M.E., Makky, A., Verasdonck, J., *et al*. (2019). Two new
663 polymorphic structures of human full-length alpha-synuclein fibrils solved by
664 cryo-electron microscopy. Elife *8*.
665
666 Guerrero-Ferreira, R., Taylor, N.M., Mona, D., Ringler, P., Lauer, M.E., Riek, R.,
667 Britschgi, M., and Stahlberg, H. (2018). Cryo-EM structure of alpha-synuclein
668 fibrils. Elife *7*.
669
670 Guo, M., Wang, J., Zhao, Y., Feng, Y., Han, S., Dong, Q., Cui, M., and Tieu, K.
671 (2020). Microglial exosomes facilitate alpha-synuclein transmission in Parkinson's
672 disease. Brain *143*, 1476-1497.
673
674 Ho, G.P.H., Ramalingam, N., Imberdis, T., Wilkie, E.C., Dettmer, U., and Selkoe,
675 D.J. (2021). Upregulation of Cellular Palmitoylation Mitigates alpha-Synuclein
676 Accumulation and Neurotoxicity. Mov Disord *36*, 348-359.
677
678 Huang, P.S., Oberdorfer, G., Xu, C., Pei, X.Y., Nannenga, B.L., Rogers, J.M.,
679 DiMaio, F., Gonen, T., Luisi, B., and Baker, D. (2014). High thermodynamic
680 stability of parametrically designed helical bundles. Science *346*, 481-485.
681
682 Jang, A., Lee, H.J., Suk, J.E., Jung, J.W., Kim, K.P., and Lee, S.J. (2010). Non-
683 classical exocytosis of alpha-synuclein is sensitive to folding states and promoted
684 under stress conditions. J Neurochem *113*, 1263-1274.
685
686 Jumper, J., Evans, R., Pritzel, A., Green, T., Figurnov, M., Ronneberger, O.,
687 Tunyasuvunakool, K., Bates, R., Zidek, A., Potapenko, A., *et al*. (2021). Highly
688 accurate protein structure prediction with AlphaFold. Nature *596*, 583-589.
689
690 Kaushik, S., and Cuervo, A.M. (2018). The coming of age of chaperone-mediated
691 autophagy. Nat Rev Mol Cell Biol *19*, 365-381.

692
693 Kim, P.K., and Hettema, E.H. (2015). Multiple pathways for protein transport to
694 peroxisomes. J Mol Biol *427*, 1176-1190.
695
696 Kim, S., Kwon, S.H., Kam, T.I., Panicker, N., Karuppagounder, S.S., Lee, S., Lee,
697 J.H., Kim, W.R., Kook, M., Foss, C.A., *et al*. (2019). Transneuronal Propagation
698 of Pathologic alpha-Synuclein from the Gut to the Brain Models Parkinson's
699 Disease. Neuron *103*, 627-641 e627.
700
701 Kordower, J.H., Chu, Y., Hauser, R.A., Freeman, T.B., and Olanow, C.W. (2008).
702 Lewy body-like pathology in long-term embryonic nigral transplants in Parkinson's
703 disease. Nat Med *14*, 504-506.
704
705 Lashuel, H.A., Petre, B.M., Wall, J., Simon, M., Nowak, R.J., Walz, T., and
706 Lansbury, P.T., Jr. (2002). Alpha-synuclein, especially the Parkinson's disease-
707 associated mutants, forms pore-like annular and tubular protofibrils. J Mol Biol
708 *322*, 1089-1102.
709
710 Lee, H.J., Patel, S., and Lee, S.J. (2005). Intravesicular localization and exocytosis
711 of alpha-synuclein and its aggregates. J Neurosci *25*, 6016-6024.
712
713 Lee, J., Xu, Y., Zhang, T., Cui, L., Saidi, L., and Ye, Y. (2018). Secretion of
714 misfolded cytosolic proteins from mammalian cells is independent of chaperone-
715 mediated autophagy. J Biol Chem *293*, 14359-14370.
716
717 Lee, J.G., Takahama, S., Zhang, G., Tomarev, S.I., and Ye, Y. (2016).
718 Unconventional secretion of misfolded proteins promotes adaptation to proteasome
719 dysfunction in mammalian cells. Nat Cell Biol *18*, 765-776.
720
721 Li, J.Y., Englund, E., Holton, J.L., Soulet, D., Hagell, P., Lees, A.J., Lashley, T.,
722 Quinn, N.P., Rehncrona, S., Bjorklund, A., *et al*. (2008). Lewy bodies in grafted
723 neurons in subjects with Parkinson's disease suggest host-to-graft disease
724 propagation. Nat Med *14*, 501-503.
725
726 Lin, D.H., and Hoelz, A. (2019). The Structure of the Nuclear Pore Complex (An
727 Update). Annu Rev Biochem *88*, 725-783.
728

729 Linder, M.E., and Deschenes, R.J. (2007). Palmitoylation: policing protein stability
730 and traffic. Nat Rev Mol Cell Biol *8*, 74-84.
731
732 Los, G.V., Encell, L.P., McDougall, M.G., Hartzell, D.D., Karassina, N., Zimprich,
733 C., Wood, M.G., Learish, R., Ohana, R.F., Urh, M., *et al*. (2008). HaloTag: a novel
734 protein labeling technology for cell imaging and protein analysis. ACS Chem Biol
735 *3*, 373-382.
736
737 Luk, K.C., Kehm, V., Carroll, J., Zhang, B., O'Brien, P., Trojanowski, J.Q., and
738 Lee, V.M. (2012). Pathological alpha-synuclein transmission initiates Parkinson-
739 like neurodegeneration in nontransgenic mice. Science *338*, 949-953.
740
741 Patel, P., Prescott, G.R., Burgoyne, R.D., Lian, L.Y., and Morgan, A. (2016).
742 Phosphorylation of Cysteine String Protein Triggers a Major Conformational
743 Switch. Structure *24*, 1380-1386.
744
745 Rapoport, T.A., Li, L., and Park, E. (2017). Structural and Mechanistic Insights
746 into Protein Translocation. Annu Rev Cell Dev Biol *33*, 369-390.
747
748 Resh, M.D. (2006). Use of analogs and inhibitors to study the functional
749 significance of protein palmitoylation. Methods *40*, 191-197.
750
751 Scheiblich, H., Dansokho, C., Mercan, D., Schmidt, S.V., Bousset, L., Wischhof,
752 L., Eikens, F., Odainic, A., Spitzer, J., Griep, A., *et al*. (2021). Microglia jointly
753 degrade fibrillar alpha-synuclein cargo by distribution through tunneling
754 nanotubes. Cell *184*, 5089-5106 e5021.
755
756 Shahmoradian, S.H., Lewis, A.J., Genoud, C., Hench, J., Moors, T.E., Navarro,
757 P.P., Castano-Diez, D., Schweighauser, G., Graff-Meyer, A., Goldie, K.N., *et al*.
758 (2019). Lewy pathology in Parkinson's disease consists of crowded organelles and
759 lipid membranes. Nat Neurosci *22*, 1099-1109.
760
761 Shurtleff, M.J., Temoche-Diaz, M.M., Karfilis, K.V., Ri, S., and Schekman, R.
762 (2016). Y-box protein 1 is required to sort microRNAs into exosomes in cells and
763 in a cell-free reaction. Elife *5*.
764
765 Stefanis, L. (2012). alpha-Synuclein in Parkinson's disease. Cold Spring Harb
766 Perspect Med *2*, a009399.

767
768 Strohaker, T., Jung, B.C., Liou, S.H., Fernandez, C.O., Riedel, D., Becker, S.,
769 Halliday, G.M., Bennati, M., Kim, W.S., Lee, S.J., *et al*. (2019). Structural
770 heterogeneity of alpha-synuclein fibrils amplified from patient brain extracts. Nat
771 Commun *10*, 5535.
772
773 Stykel, M.G., Humphries, K.M., Kamski-Hennekam, E., Buchner-Duby, B., Porte-
774 Trachsel, N., Ryan, T., Coackley, C.L., Bamm, V.V., Harauz, G., and Ryan, S.D.
775 (2021). alpha-Synuclein mutation impairs processing of endomembrane
776 compartments and promotes exocytosis and seeding of alpha-synuclein pathology.
777 Cell Rep *35*, 109099.
778
779 Virlogeux, A., Scaramuzzino, C., Lenoir, S., Carpentier, R., Louessard, M.,
780 Genoux, A., Lino, P., Hinckelmann, M.V., Perrier, A.L., Humbert, S., *et al*. (2021).
781 Increasing brain palmitoylation rescues behavior and neuropathology in
782 Huntington disease mice. Sci Adv *7*.
783
784 Xu, Y., Cui, L., Dibello, A., Wang, L., Lee, J., Saidi, L., Lee, J.G., and Ye, Y.
785 (2018). DNAJC5 facilitates USP19-dependent unconventional secretion of
786 misfolded cytosolic proteins. Cell Discov *4*, 11.
787
788 Yim, N., Ryu, S.W., Choi, K., Lee, K.R., Lee, S., Choi, H., Kim, J., Shaker, M.R.,
789 Sun, W., Park, J.H., *et al*. (2016). Exosome engineering for efficient intracellular
790 delivery of soluble proteins using optically reversible protein-protein interaction
791 module. Nat Commun *7*, 12277.
792
793 Zacharias, D.A., Violin, J.D., Newton, A.C., and Tsien, R.Y. (2002). Partitioning
794 of lipid-modified monomeric GFPs into membrane microdomains of live cells.
795 Science *296*, 913-916.
796
797 Zhang, M., Liu, L., Lin, X., Wang, Y., Li, Y., Guo, Q., Li, S., Sun, Y., Tao, X.,
798 Zhang, D., *et al*. (2020). A Translocation Pathway for Vesicle-Mediated
799 Unconventional Protein Secretion. Cell *181*, 637-652 e615.
800
801 Zhang, Y.Q., and Chandra, S.S. (2014). Oligomerization of Cysteine String Protein
802 alpha mutants causing adult neuronal ceroid lipofuscinosis. Biochim Biophys Acta
803 *1842*, 2136-2146.
804

805 Zinsmaier, K.E. (2010). Cysteine-string protein's neuroprotective role. J
806 Neurogenet *24*, 120-132.

807

808 ## Figure legends

809 **Figure 1.** Reconstitution of α-syn secretion regulated by palmitoylated DNAJC5
810 in HEK293T cells.

811 (A) Schematic diagrams of α-syn and DNAJC5. Domains are highlighted in
812 different colors. Red arrows indicate known disease-causing mutations on each
813 protein.
814 (B) Membrane and cytosol fractionation scheme. Briefly, homogenized
815 HEK293T cells were centrifuged at low speed to prepare a post-nuclear
816 supernatant (PNS). High-speed centrifugation was then performed to separate
817 the insoluble membrane (M) from cytosol (C).
818 (C) Partition of palmitoylated DNAJC5 (P-DNAJC5) and non-palmitoylated
819 DNAJC5 (NP-DNAJC5) between the membrane (M) and cytosol (C) fractions.
820 DNAJC5 was immunoprecipitated from cytosol and membrane with anti-FLAG
821 resin and evaluated by Coomassie-blue stained SDS-PAGE.
822 (D) α-syn secretion 16 h after transfection. The secretion of P-DNAJC5 in the
823 medium was detected.
824 (E) α-syn secretion 36 h after transfection. NP-DNAJC5 was also secreted in the
825 medium together with α-syn.

826 **Figure 1 – figure supplement 1**. Secretion of α-syn variants. HEK293T cells were
827 co-transfected with Parkinson's disease (PD)-causing α-syn mutant (A30P, E46K,
828 A53T) and DNAJC5.

829 (A) Secretion of α-syn variants into conditioned medium. Medium was
830 collected, concentrated and evaluated by immunoblot.
831 (B) Expression of α-syn variants in HEK293T cells.

832 **Figure 1 – figure supplement 2.** Basal secretion of α-syn is partially dependent
833 on endogenous DNAJC5.

834 (A) Schematic diagram of Nanoluciferase (Nluc)-fused α-syn.
835 (B) Nluc-α-syn secretion was stimulated by DNAJC5 expression. Plasmids
836 encoding Nluc-α-syn and DNAJC5 were co-transfected into HEK293T cells.
837 Expression and secretion of proteins were detected with immunoblot 36 h after
838 transfection.
839 (C) Time-dependent of accumulation of Nluc-α-syn in the medium without
840 DNAJC5 overexpression. After transfecting HEK293T cells with Nluc-α-syn
841 alone, fractions of medium were collected at indicated time points.
842 (D) Chemical structure of Quercetin (QLT), a reported DNAJC5 inhibitor.
843 (E) QLT inhibited endogenous Nluc-α-syn secretion in a concentration-
844 dependent manner. AU, arbitrary unit. Secretion assay similar to (B) was
845 performed with treatment of indicated concentration of QLT. Amounts of
846 secreted proteins were quantified with nanoluciferase assay 36hr after
847 transfection.
848 (F) HEK293T cells were co-transfected with Nluc-α-syn and siRNA targeting
849 DNAJC5. At 36 h post transfection, cells were harvested for testing knockdown
850 (KD) efficiency by immunoblot.
851 (G) Nluc-α-syn secretion decreased in DNAJC5 KD cells compared with
852 control.

853 **Figure 2.** Characterization of secreted α-syn.

854 (A) Medium fractionation scheme.

855 (B) Secreted α-syn was soluble. Differential centrifugation was performed with
856 conditioned medium from HEK293T cells transfected with DNAJC5 and α-
857 syn. Alix and CD9, exosome markers. PDI, an endoplasmic reticulum (ER)
858 marker, was used as exosome-negative marker.

859 (C) Gel filtration fractionation of medium. Conditioned medium was
860 concentrated and subjected to gel filtration fractionation. Fractions were
861 evaluated by anti-α-syn immunoblot.

862 (D) Chromatograms of tandem α-syn monomer (blue curve), dimer (green
863 curve) and tetramer (red curve) were overlaid. In comparison, the relative
864 intensity of secreted α-syn in each fraction was plotted as blue bars.

865 (E) Schematic diagram of co-immunoprecipitation (co-IP) of secreted α-syn and
866 FLAG-α-syn. Shown here is possible interaction between α-syn (blue circle)
867 and FLAG-α-syn (yellow circle) in a representative tetrameric conformation.

868 (F) Anti-FLAG Immunoprecipitation (FLAG-IP) of media from cells transfected
869 with indicated plasmids. Both the medium input and FLAG-IP samples were
870 evaluated with anti-α-syn immuno(western)blot (anti-α-syn WB).

871 **Figure 2 – figure supplement 1**. Solubility of secreted α-syn variants.

872 (A) Medium fractionation of secreted α-syn PD mutants (A30P, E46K and
873 A53T). After differential centrifugation of medium, supernatant (10ks and
874 100ks) and pellet fractions (100kp) were evaluated by immunoblot.

875 (B) Medium fractionation of basal secreted Nluc-α-syn without DNAJC5
876 overexpression. Similar fractionation assay was performed in (A) with medium
877 from HEK293T cells transfected with Nluc-α-syn alone. Secreted Nluc-α-syn
878 was quantified with nanoluciferase assay. AU, arbitrary unit.

879 **Figure 2- figure supplement 2.** DNAJC5 enriched in buoyant EV fraction.

880 (A) Schematic diagram of EV flotation protocol. Briefly, high-speed pellet
881 fractions of growth medium were resuspended in 60% sucrose buffer and
882 overlaid sequentially with 40% and 10% sucrose buffer. The tubes were
883 centrifuged at 150,000 (150k)xg at 4°C for overnight. Buoyant EVs floated at
884 the 10%/40% sucrose interface, separated from other insoluble materials.
885 (B) Immunoblots across the sucrose step gradient. DNAJC5 as well as other
886 classical exosome markers (Flot-2, CD63 and CD9) were highly enriched in
887 fractions 4 to 6 at the 10%/40% interface.

888 **Figure 2 – figure supplement 3**. Assessment of tandem α-syn oligomers by gel
889 filtration chromatography.

890 (A) Chromatogram of purified tetrameric α-syn tandem oligomer (α-syn-α-syn-
891 α-syn-α-syn).
892 (B) Coomassie-blue stained SDS-PAGE of fractions from gel filtration of
893 tetrameric α-syn tandem oligomer (α-syn-α-syn-α-syn-α-syn).
894 (C) Chromatogram of purified dimeric α-syn tandem oligomer (α-syn-α-syn).
895 (D) Coomassie-blue stained SDS-PAGE of fractions from gel filtration of
896 dimeric α-syn tandem oligomer (α-syn-α-syn).
897 (E) Chromatogram of purified WT α-syn (α-syn).

898 (F) Coomassie-blue stained SDS-PAGE of fractions from gel filtration of
899 WT α-syn (α-syn).

900

901

902 **Figure 3**. Disruption of palmitoylation of DNAJC5 inhibited α-syn secretion.
903 (A) Inhibition of DNAJC5 palmitoylation by 2-bromopalmitic acid (2-BA) or
904 introduced mutation L115R. Cellular fractionation was performed with
905 HEK293T cells transfected with WT DNAJC5 and treated with 10 μm 2-BA, or
906 transfected with DNAJC5 L115R mutant. TFR, transferrin receptor. PNS, post-
907 nuclear supernatant. C, cytosol. M, membrane.
908 (B) α-syn secretion was blocked with 2-BA treatment. HEK293T cells
909 transfected with indicated plasmids were treated with DMSO or 10 μm 2-BA.
910 Media were collected and secretion was evaluated by SDS PAGE and
911 immunoblot.
912 (C) Palmitoylation of DNAJC5 was blocked in HEK293T cells treated with 2-
913 BA.
914 (D) DNAJC5 L115R mutant reduced α-syn secretion compared with WT
915 DNAJC5. Secretion assay with HEK293T cells transfected with indicated
916 plasmids encoding DNAJC5 variant was performed similar to (B).
917 (E) DNAJC5 L115R was non-palmitoylated in HEK293T cells.

918 **Figure 3 – figure supplement 1**. Dose-dependent inhibition of α-syn secretion by
919 2-bromopalmitic acid (2-BA).

920 (A) Chemical structure of palmitoylation inhibitor 2-bromopalmitic acid (2-BA).
921 The single bromo substituent at position 2 is highlighted by a red dashed
922 square.
923 (B) α-syn secretion in the medium was inhibited by 2-BA in a dose-dependent
924 manner. Ten μm 2-BA was serially diluted by DMSO into 5 μm, 2μm, 1μm
925 solution. HEK293T cells were first transfected with DNAJC5 and α-syn. After
926 medium replacement, 2-BA of indicated concentration was added to cell
927 culture. Media was collected after 36h and followed by sample preparation,
928 SDS PAGE and immunoblot.
929 (C) With increasing concentration of 2-BA, P-DNAJC5 decreased and NP-
930 DNAJC5 increased in HEK293T cells.

931 **Figure 3 – figure supplement 2.** Blockage of USP19-induced α-syn secretion by
932 DNAJC5 L115R or L116Δ mutant.

933 (A) USP19 induced α-syn secretion in the medium, which was further enhanced
934 by WT DNAJC5 and blocked by two DNAJC5 palmitoylation-deficient
935 mutants (L115R and L116Δ).
936 (B) Both mutations, L115R and L115Δ, inhibited DNAJC5 palmitoylation in
937 HEK293T cells.

938 **Figure 4**. Topological localization of α-syn and DNAJC5 in enlarged endosomes.

939 (A) DNAJC5 was internalized inside enlarged endosomes. Live U2OS cells
940 expressing mCherry-Rab5^{Q79L} (red) showed circular enlarged endosomes
941 labeled by Rab5 mutant. DNAJC5-HaloTag (green) was visualized by addition
942 of HaloTag® Oregon Green® Ligand. Representative enlarged endosomes show

943 diffuse (1) or punctate (2 and 3) internalized DNAJC5. Scale bar: 15 μm in
944 overviews and 1 μm in magnified insets.
945 (B) α-syn was excluded from enlarged endosomes. In live U2OS cells,
946 expression of BFP-Rab5^{Q79L} (blue) produced enlarged endosomes of similar
947 morphology compared with mCherry-Rab5^{Q79L}. mNeonGreen-α-syn (mNG-α-
948 syn, green) was expressed both in the nucleus and cytosol. No mNG-α-syn was
949 found inside enlarged endosomes (1, 2, 3). Scale bar: 20 μm in overviews and 1
950 μm in magnified insets.
951 (C) α-syn enters into enlarged endosomes in the presence of DNAJC5. DNAJC5-
952 HaloTag (red) and mNG-α-syn (green) were co-expressed in U2OS cells
953 carrying BFP-Rab5^{Q79L} (blue) mutant and imaged. No mNG-α-syn was
954 internalized in endosome without DNAJC5-HaloTag inside (1). In contrast,
955 mNG-α-syn was found inside endosomes with DNAJC5-HaloTag inside (2 and
956 3). Scale bar: 10 μm in overviews and 1 μm in magnified insets.
957 (D) α-syn and DNAJC5 co-fractionated in membrane fractionation. HEK293T
958 cell homogenate was sequentially centrifuged at increasing velocity from 3000g
959 (3k), 25,000g (25k) and 100,000g (100k). The 25k membrane fraction had the
960 highest amount of both α-syn and DNAJC5.
961 (E) Proteinase K protection assay of 25k membrane containing α-syn and
962 DNAJC5.
963

964 **Figure 4 – figure supplement 1**. Immunofluorescence (IF) images of endogenous
965 DNAJC5 and enlarged endosomes.

966 (A) Co-localization between endogenous CD63 (red) and DNAJC5 (green).
967 U2OS cells were cultured and fixed, incubated with corresponding antibodies
968 for IF detection of endogenous CD63 and DNAJC5. Representative co-
969 localized region is shown in magnified insets. Scale bar, 20 μm.
970 (B) CD63 (green) was inside the enlarged endosomes labeled by peripheral
971 mCherry-Rab5^{Q79L} (red). U2OS expressing mCherry-Rab5^{Q79L} were fixed,
972 followed by IF using anti-CD63 antibody. Scale bar, 25 μm.

973 **Figure 4 – figure supplement 2**. Live-cell images of U2OS cells expressing
974 DNAJC5 L115R mutant and α-syn.

975 (A) Live cell imaging of U2OS cells transfected with DNAJC5 (L115R)-
976 HaloTag and mCherry-Rab5^{Q79L}. DNAJC5 (L115R)-HaloTag (green) is diffuse
977 in cytosol and outside of the enlarged endosomes labeled by peripheral
978 mCherry-Rab5^{Q79L} (red). Scale bar, 10 μm in overviews and 1 μm in magnified
979 insets.
980 (B) Live cell imaging of U2OS cells transfected with mNeonGreen (mNG)-α-
981 syn, DNAJC5 (L115R)-HaloTag and mCherry-Rab5^{Q79L}. In the condition of
982 co-expression with DNAJC5 (L115R)-HaloTag (red), no mNG-α-syn (green)
983 was found inside of enlarged endosomes labeled by peripheral BFP-Rab5^{Q79L}
984 (blue). Scale bar, 10 μm in overviews and 1 μm in magnified insets.

985 **Figure 4 - supplement video**. Time lapse of movement of internalized α-syn and
986 DNAJC5 in the enlarged endosomes. DNAJC5-HaloTag (red) and mNG-α-syn
987 (green) were co-expressed in U2OS cells carrying BFP-Rab5^{Q79L} (blue) mutant and
988 imaged. Scale bar: 10 μm.

989 **Figure 5**. Secretion of tandem α-syn oligomers and α-syn fused with thermostable
990 helix bundle protein.
991 (A) Schematic diagrams of tandem α-syn oligomers. α-syn protomers (yellow)
992 were linked head to tail by flexible linker (green) to mimic increased size of α-
993 syn oligomers.
994 (B) Secretion of tandem α-syn oligomers in medium. Secretion assay was
995 performed with media from HEK293T cells culture transfected with indicated
996 tandem α-syn oligomers. Tandem α-syn oligomers are more sensitively
997 detected by immunoblot and were exposed for shorter time compared with WT
998 α-syn.
999 (C) Expression of tandem α-syn oligomers in HEK293T cells. *a non-specific
1000 band.
1001 (D) Schematic diagrams of N-terminal fused and C-terminal fused thermostable
1002 three helix bundle (3H-) α-syn. 3H was shown as three blue dashes, α-syn was
1003 shown as orange circle.
1004 (E) Secretion of 3H-SYN and SYN-3H in medium. Secretion assay was
1005 performed with media from HEK293T cells culture transfected with indicated
1006 3H-fused α-syn constructs. *a non-specific band.
1007 (F) Expression of 3H-SYN and SYN-3H in HEK293T cells. *a non-specific
1008 band.

1009 **Figure 5 – figure supplement**. Medium fractionation of secreted tandem α-syn
1010 oligomers.

1011 **Figure 6.** XPACK (XP)-induced DNAJC5 L115R oligomerization rescued α-syn
1012 secretion.

1013 (A) Ladder pattern of higher molecular weight (HMW) DNAJC5 oligomers in
1014 the medium. Medium from HEK293T cell culture transfected with DNAJC5
1015 was centrifuged at 1000 (1k) g, 10,000 (10k) g and 100,000 (100k) g, followed
1016 by immunoblot of supernatants (s) at each centrifugation step.
1017 (B) Fractionation of HMW-DNAJC5 with gel filtration. HEK293T cells
1018 transfected with DNAJC5 were lysed, clarified and subjected to gel filtration.
1019 HMW-DNAJC5 of different sizes were separated based on their corresponding
1020 molecular weight.
1021 (C) XP-DNAJC5 L115R mutant forms a membrane-bound oligomer. Cellular
1022 fractionation was performed with HEK293T cells transfected with indicated
1023 DNAJC5 variants. Note the substantial change of electrophoretic mobility of
1024 XP-DNAJC5 L115R on SDS-PAGE.
1025 (D) α-syn secretion induced by XP-DNAJC5 L115R. Secretion assay was
1026 performed with HEK293T cells transfected with indicated plasmids. Ten μm 2-
1027 BA was used to block induced α-syn.
1028 (E) Expression of α-syn and DNAJC5 variants in HEK293T cells. Note the
1029 substantial change in electrophoretic mobility of 2-BA-treated XP-DNAJC5
1030 L115R on SDS-PAGE.

1031 **Figure 6 – figure supplement 1**. Characterization of HMW-DNAJC5 and
1032 XPACK fusion.

1033 (A) DNAJC5 (ΔJ) forms a series of SDS-resistant oligomers. HEK293T cells
1034 transfected with WT DNAJC5 or DNAJC5 (ΔJ) were lysed and evaluated by
1035 immunoblot using anti-DNAJC5 antibody.

1036 (B) HMW-DNAJC5 is not formed by non-specific disulfide bonds. HEK293T
1037 cells transfected with DNAJC5 were lysed for SDS-PAGE followed by
1038 immunoblot. The loading samples for SDS-PAGE were prepared with
1039 increasing amount of DTT up to 40 mM.
1040 (C) Schematic diagram of XPACK. XPACK is myristoylated on the first glycine
1041 (G) and palmitoylated on the second cystine (C). Replacement of Serine (S) at
1042 position 5 with a hydrophobic isoleucine (I) abolishes normal lipidation of
1043 XPACK.
1044 (D) Assessment of different XPACK fusion constructs. Cell lysate containing
1045 different DNAJC5 constructs were evaluated by anti-DNAJC5 immunoblot.
1046 (E) Membrane-association of XP-DNAJC5 dependent on palmitoylation.
1047 HEK293T cells transfected with XP-DNAJC5 were treated with DMSO or 10
1048 μM 2-BA. After cell culture for 24 h, cellular fractionation was performed with
1049 homogenized cells. Distribution of XP-DNAJC5 in cytosol (C) and membrane
1050 (M) fractions were evaluated with immunoblot.

1051 **Figure 6 – figure supplement 2**. Live-cell images of U2OS cells expressing XP-
1052 DNAJC5 L115R mutant and α-syn.

1053 (A) Internalization of punctate XP-DNAJC5 (green) into enlarged endosomes
1054 labeled by mCherry-Rab5^{Q79L} (red). U2OS cells were transfected with XP-
1055 DNAJC5 and mCherry-Rab5^{Q79L}. Live cell imaging was performed 24 h after
1056 transfection. Representative enlarged endosomes with XP-DNAJC5 are shown
1057 in magnified inset. Scale bar: 10 μm in overviews and 1 μm in magnified
1058 insets.
1059 (B) α-syn enters into enlarged endosomes in the presence of XP-DNAJC5. XP-
1060 DNAJC5-HaloTag (red) and mNG-α-syn (green) were co-expressed in U2OS

1061 cells carrying BFP-Rab5^{Q79L} (blue) mutant and imaged. Representative enlarged
1062 endosome with both XP-DNAJC5-HaloTag and mNG-α-syn inside is shown in
1063 magnified inset. Scale bar: 10 μm in overviews and 1 μm in magnified insets.
1064

1065 **Figure 7**. Domain mapping of secretion-competent DNAJC5.

1066 (A) Predicted structure of DNAJC5 by AlphaFold. Color scheme: J domain
1067 (magenta), Cys string domain (yellow) and C-terminal helix (green).
1068 (B) DNAJC5 (ΔJ) was competent to induce α-syn secretion into the medium.
1069 HEK293T cells were transfected with indicated plasmids. Media were collected
1070 after 36 h and evaluated with immunoblot.
1071 (C) DNAJC5 (ΔJ) formed oligomers in HEK293T cells.
1072 (D) C-terminal truncated DNAJC5 constructs were competent to induce α-syn
1073 secretion in the medium. HEK293T cells were transfected with C-terminal
1074 truncated DNAJC5 and α-syn. DNAJC5 antibodies cannot recognize DNAJC5
1075 (ΔC30) and DNAJC5 (ΔC40) because of a missing epitope in the C-terminus.
1076 Instead, DNAJC5 (ΔC30) and DNAJC5 (ΔC40) were detected by C-terminal
1077 FLAG tags. All the C-terminal truncated DNAJC5 constructs showed smear-
1078 like oligomers.
1079 (E) Expression of C-terminal truncated DNAJC5 constructs inside of HEK293T
1080 cells. Immunoblot of anti-FLAG antibody and anti-DNAJC5 antibody cross-
1081 validated the existence of oligomers.
1082 (F) A model for palmitoylated DNAJC5 oligomer-mediated α-syn secretion.

1083

1084

1085 **Figure 1 – source data**. Uncropped immunoblot and gel images corresponding to
1086 Figure 1.

1087 **Figure 1 – figure supplement 1 – source data**. Uncropped immunoblot images
1088 corresponding to Figure 1 supplement 1.

1089 **Figure 1 – figure supplement 2 – source data**. Uncropped immunoblot images
1090 corresponding to Figure 1 supplement 2.

1091 **Figure 2 – source data**. Uncropped immunoblot corresponding to Figure 2.

1092 **Figure 2 – figure supplement 1 – source data**. Uncropped immunoblot images
1093 corresponding to Figure 2 supplement 1.

1094 **Figure 2 – figure supplement 2 – source data**. Uncropped immunoblot images
1095 corresponding to Figure 2 supplement 2.

1096 **Figure 2 – figure supplement 3 – source data**. Uncropped gel images
1097 corresponding to Figure 2 supplement 3.

1098 **Figure 3 – source data**. Uncropped immunoblot corresponding to Figure 3.

1099 **Figure 3 – figure supplement 1 – source data**. Uncropped immunoblot
1100 corresponding to Figure 3 supplement 1.

1101 **Figure 3 – figure supplement 2 – source data**. Uncropped immunoblot
1102 corresponding to Figure 3 supplement 2.

1103 **Figure 4 – source data**. Uncropped immunoblot corresponding to Figure 4.

1104 **Figure 5 – source data**. Uncropped immunoblot corresponding to Figure 5.

1105 **Figure 5 – figure supplement – source data**. Uncropped immunoblot
1106 corresponding to Figure 5 supplement.

1107 **Figure 6 – source data**. Uncropped immunoblot corresponding to Figure 6.

1108 **Figure 6 – figure supplement 1 – source data**. Uncropped immunoblot
1109 corresponding to Figure 6 supplement 1.

1110 **Figure 7 – source data**. Uncropped immunoblot corresponding to Figure 7.

1111

1112

1113

1114

1115

1116

1117

1118

1119

1120

1121

1122 **Figure 1.** Reconstitution of α-syn secretion regulated by palmitoylated DNAJC5

1123 in HEK293T cells.

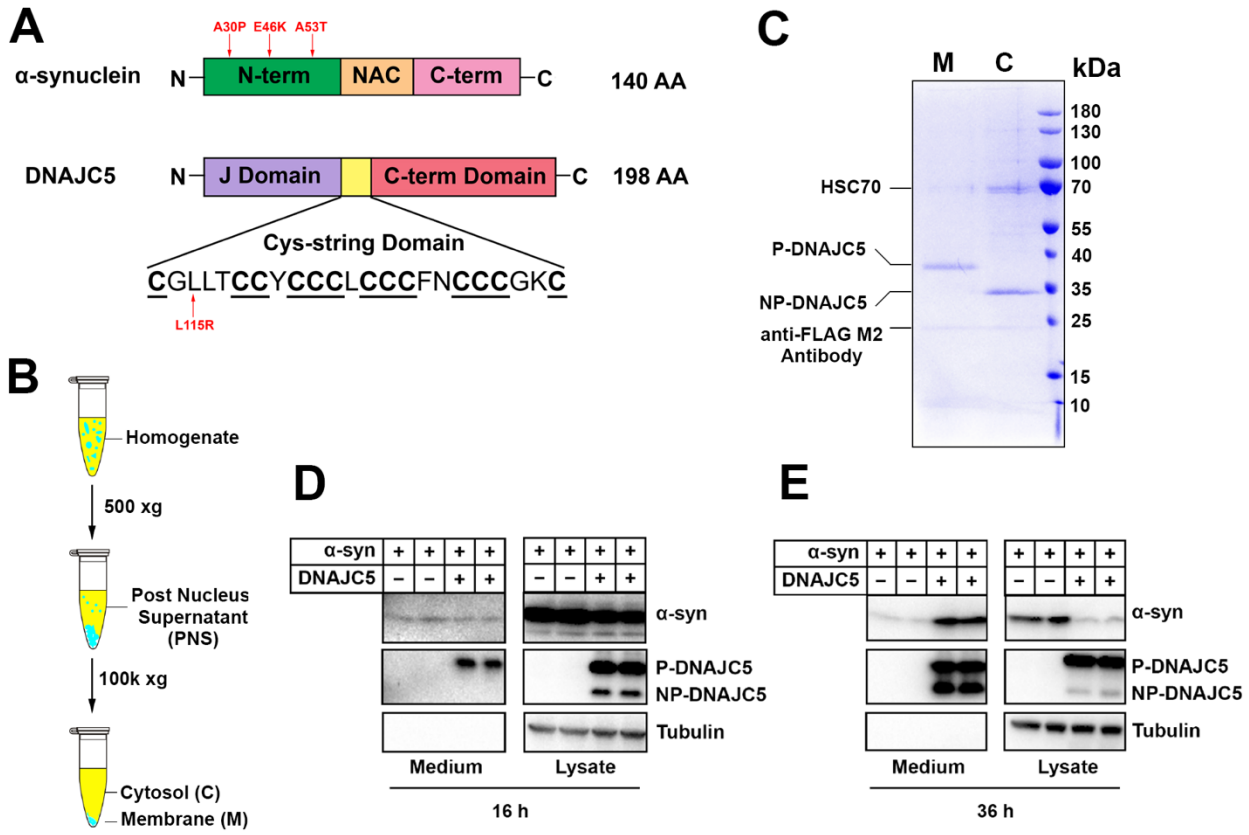

1124

1125

1126 **Figure 1 – figure supplement 1**. Secretion of α-syn variants.

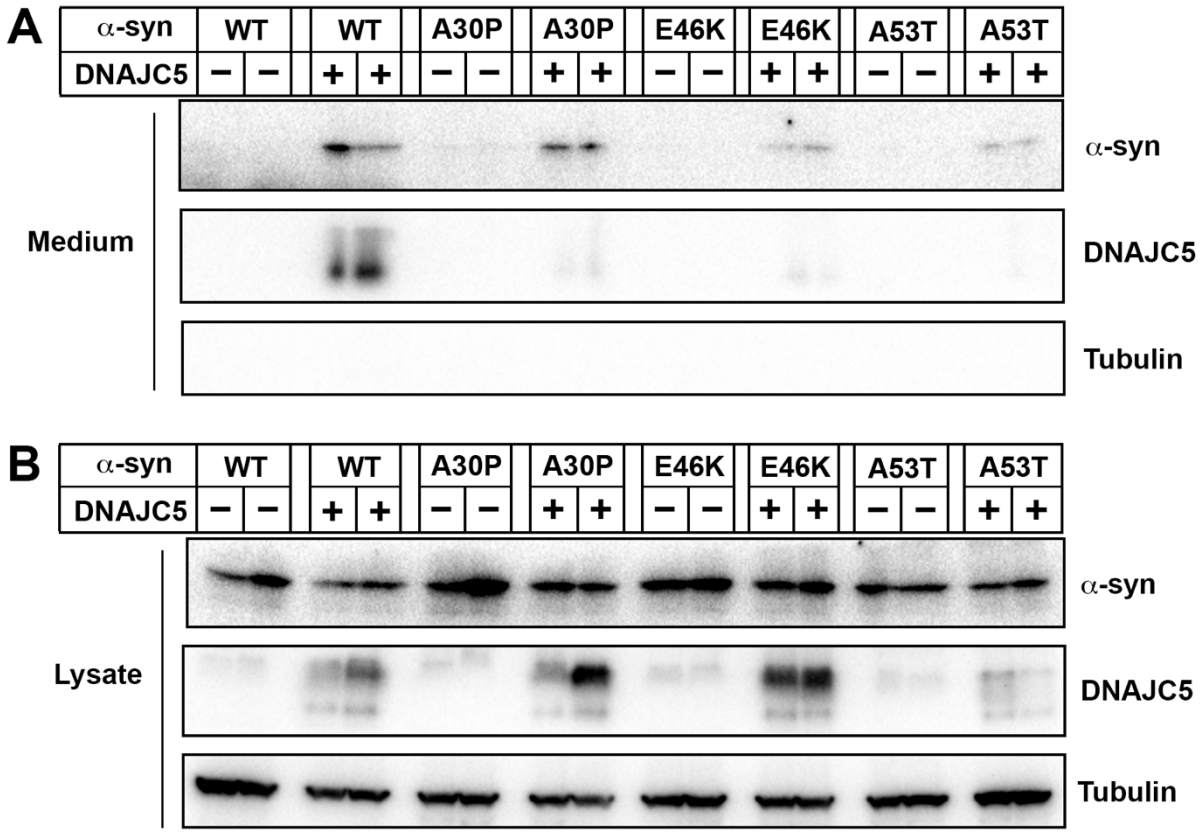

1127

1128 **Figure 1 – figure supplement 2.** Basal secretion of α-syn is partially dependent

1129 on endogenous DNAJC5.

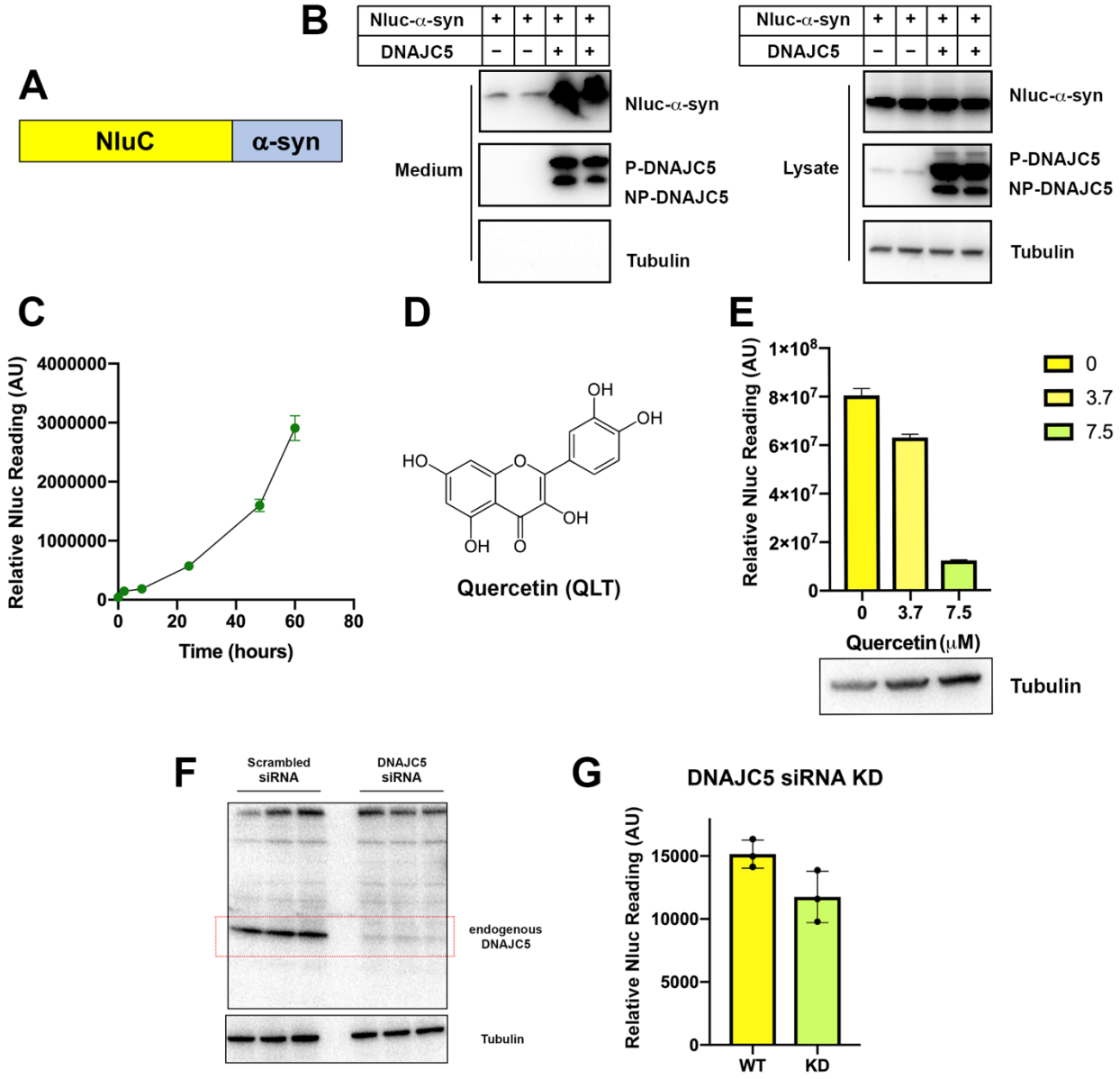

1130

1131

1132 **Figure 2.** Characterization of secreted α-syn.

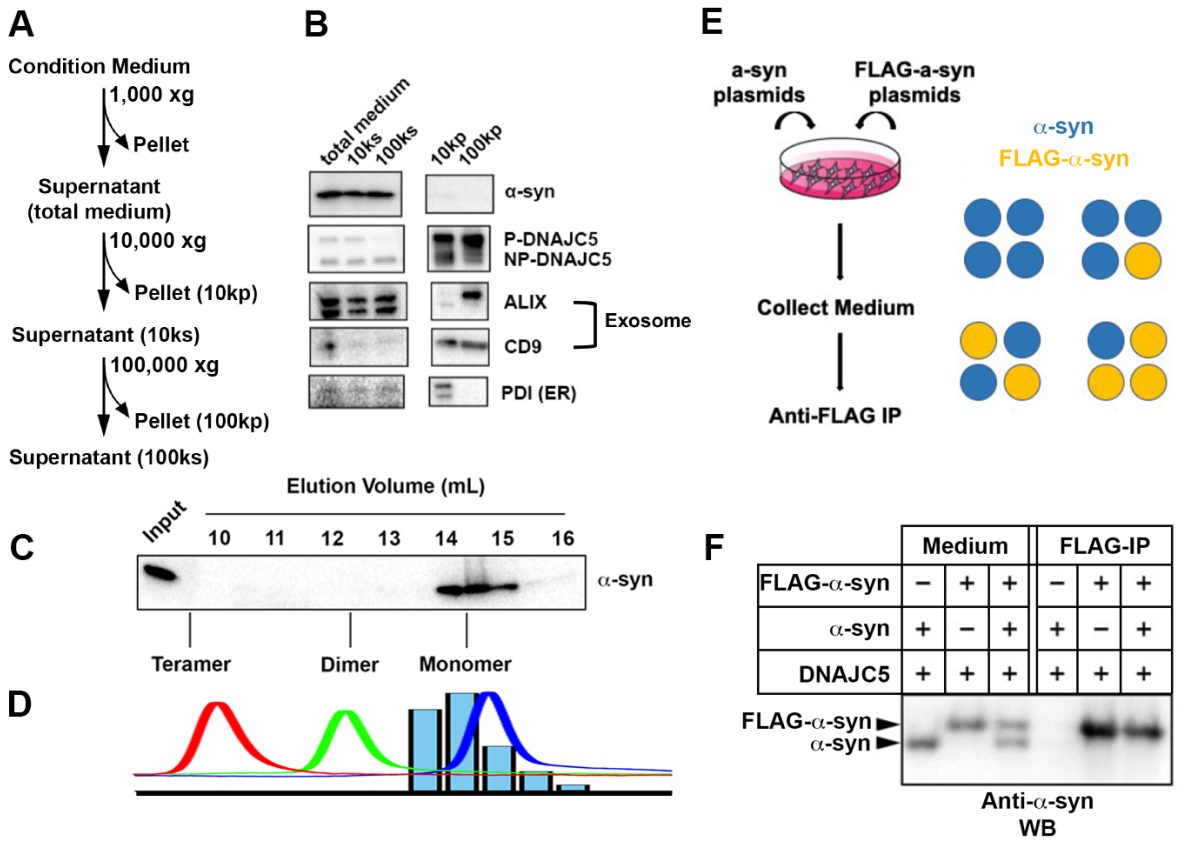

1133

1134

1135 **Figure 2 – figure supplement 1**. Solubility of secreted α-syn variants.

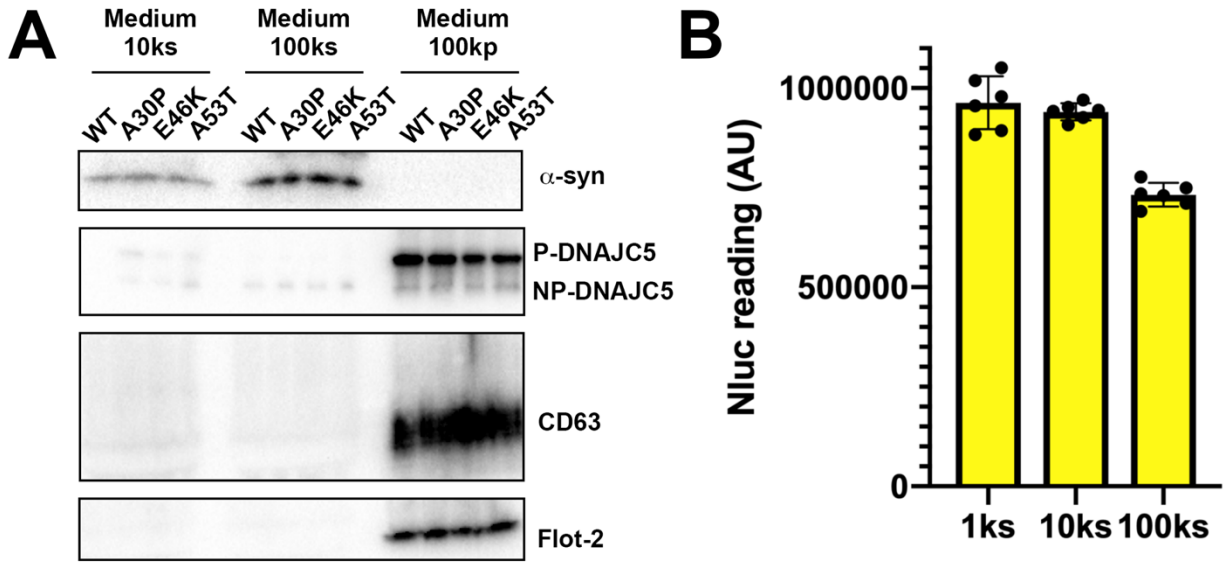

1136

1137

1138

1139 **Figure 2- figure supplement 2.** DNAJC5 enriched in buoyant EV fraction.

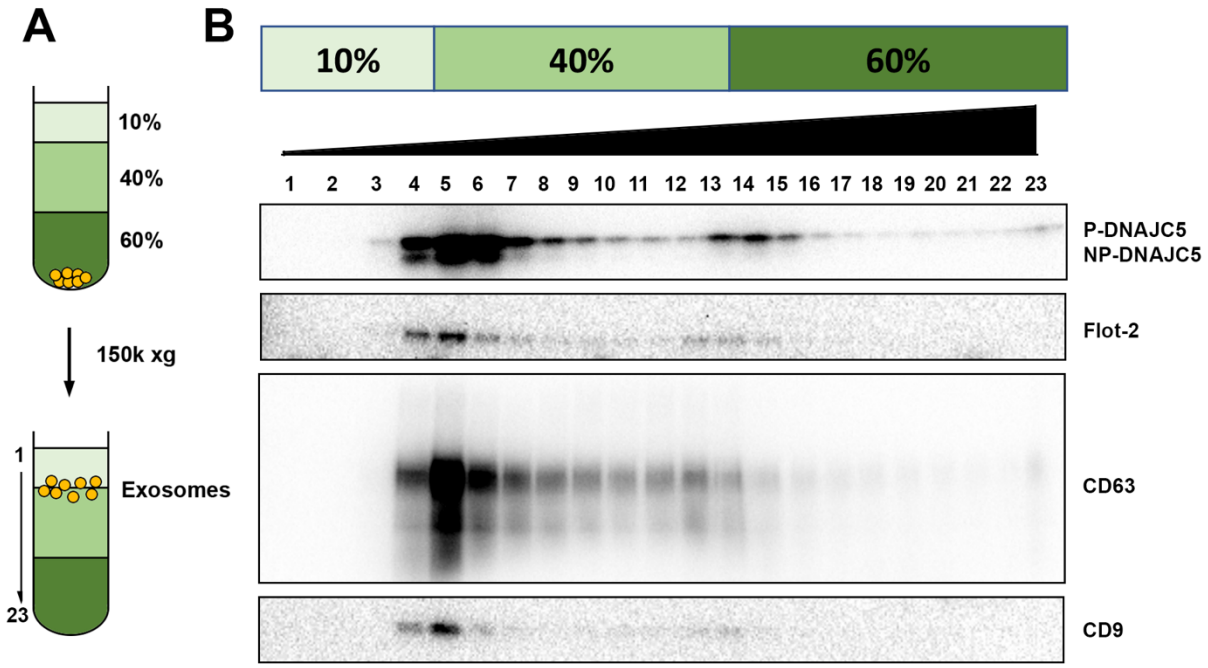

1140

1141

1142 **Figure 2 – figure supplement 3**. Assessment of tandem α-syn oligomers with gel

1143 filtration chromatography.

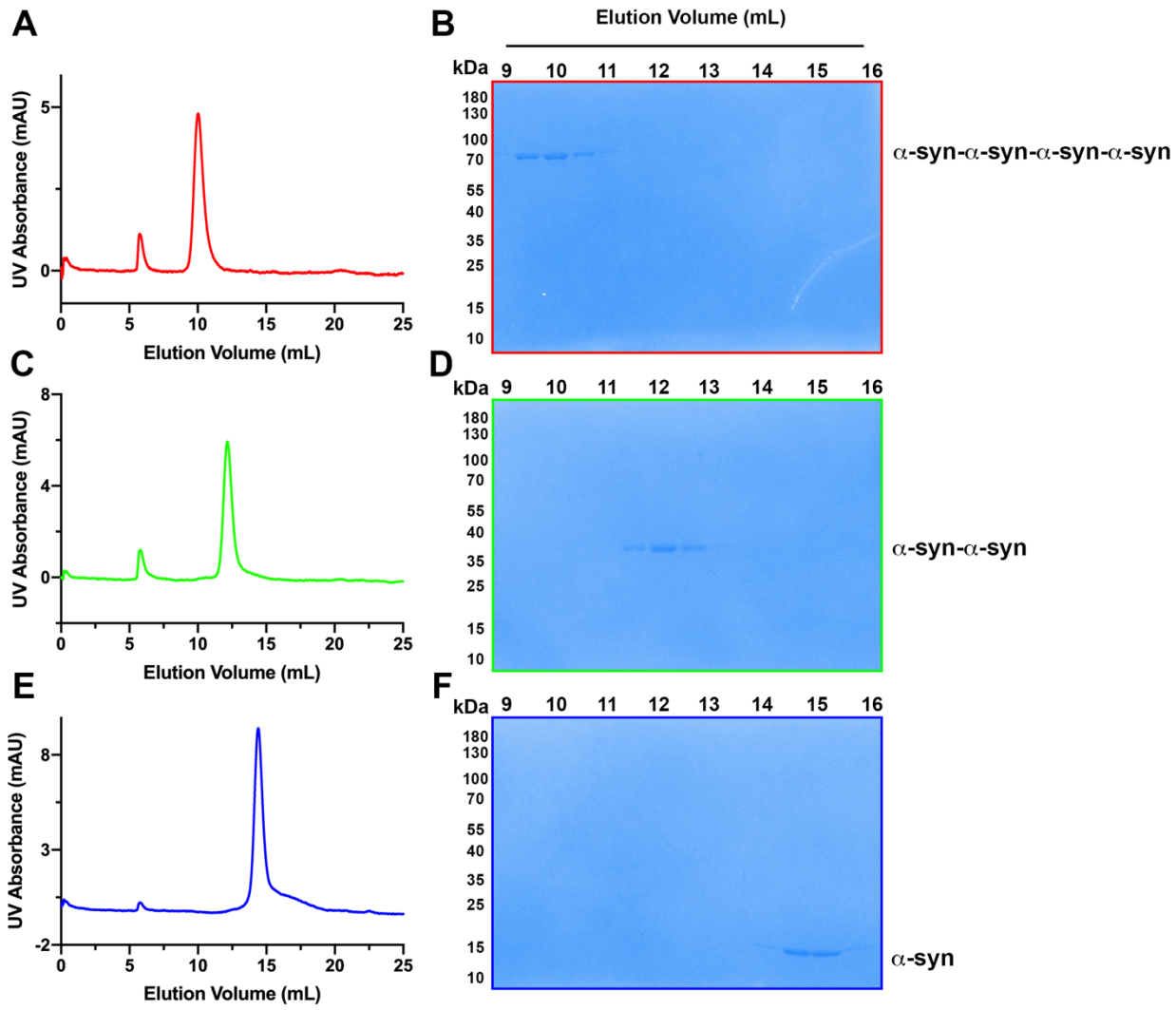

1144

1145

1146 **Figure 3**. Disruption of palmitoylation of DNAJC5 inhibited α-syn secretion.

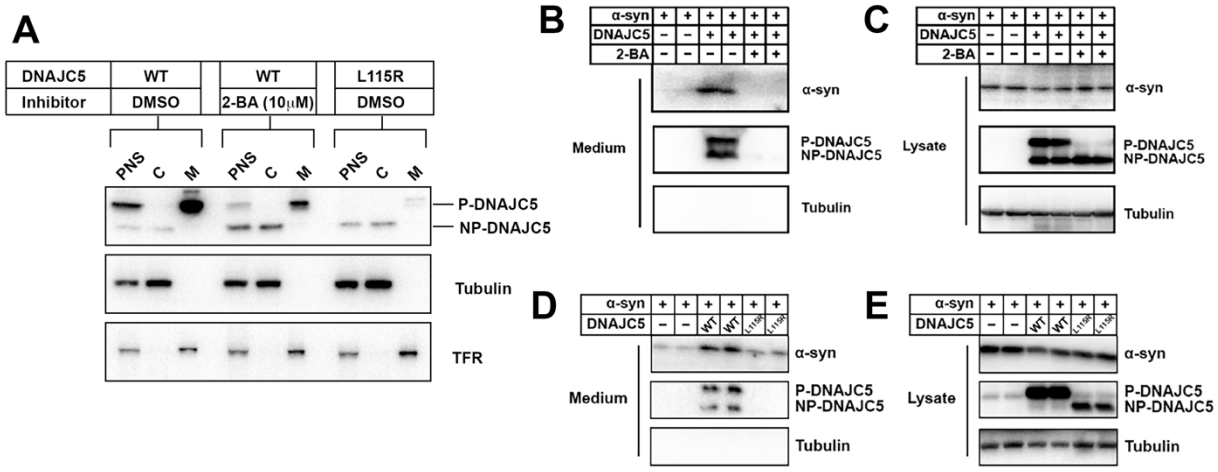

1147

1148

1149 **Figure 3 – figure supplement 1**. Dose-dependent inhibition of α-syn secretion by

1150 2-bromopalmitic acid (2-BA).

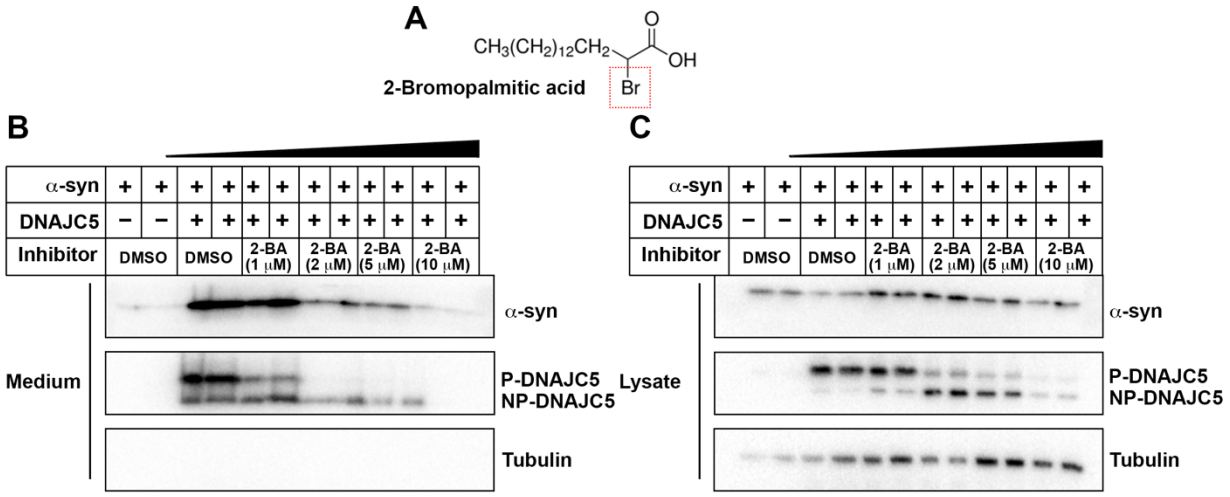

1151

1152

1153 **Figure 3 – figure supplement 2.** Blockage of USP19-induced α-syn secretion by

1154 DNAJC5 L115R or L116Δ mutant.

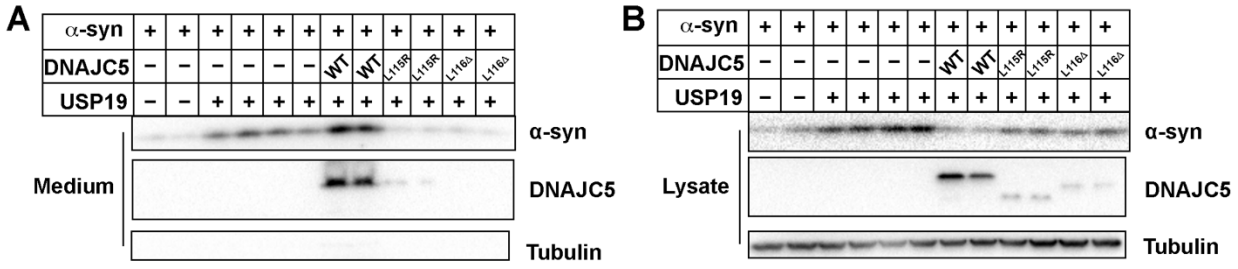

1155

1156

1157 **Figure 4**. Topological localization of α-syn and DNAJC5 in enlarged endosomes.

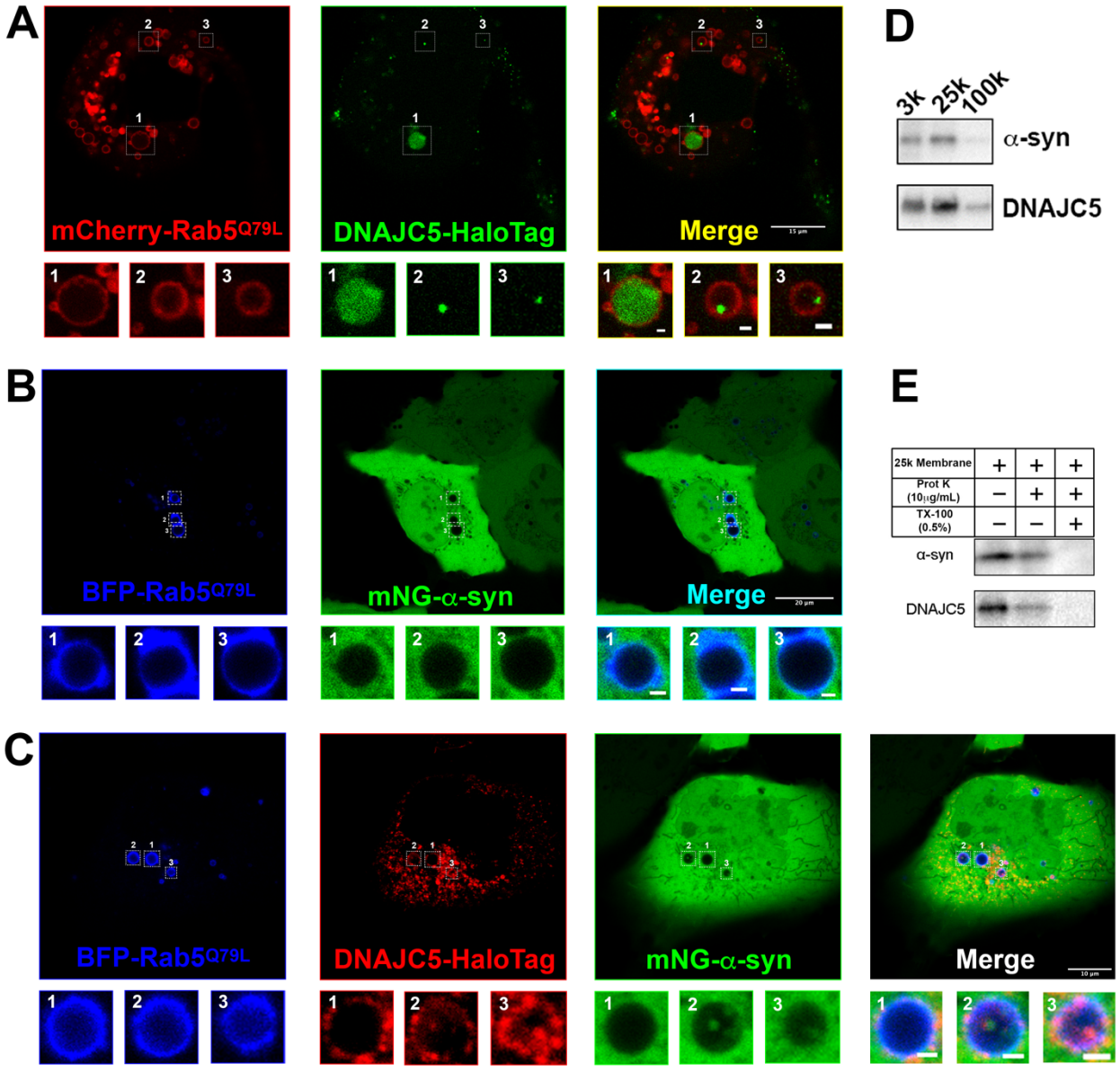

1158

1159

1160 **Figure 4 – figure supplement 1**. Immunofluorescence (IF) images of endogenous

1161 DNAJC5 and enlarged endosomes.

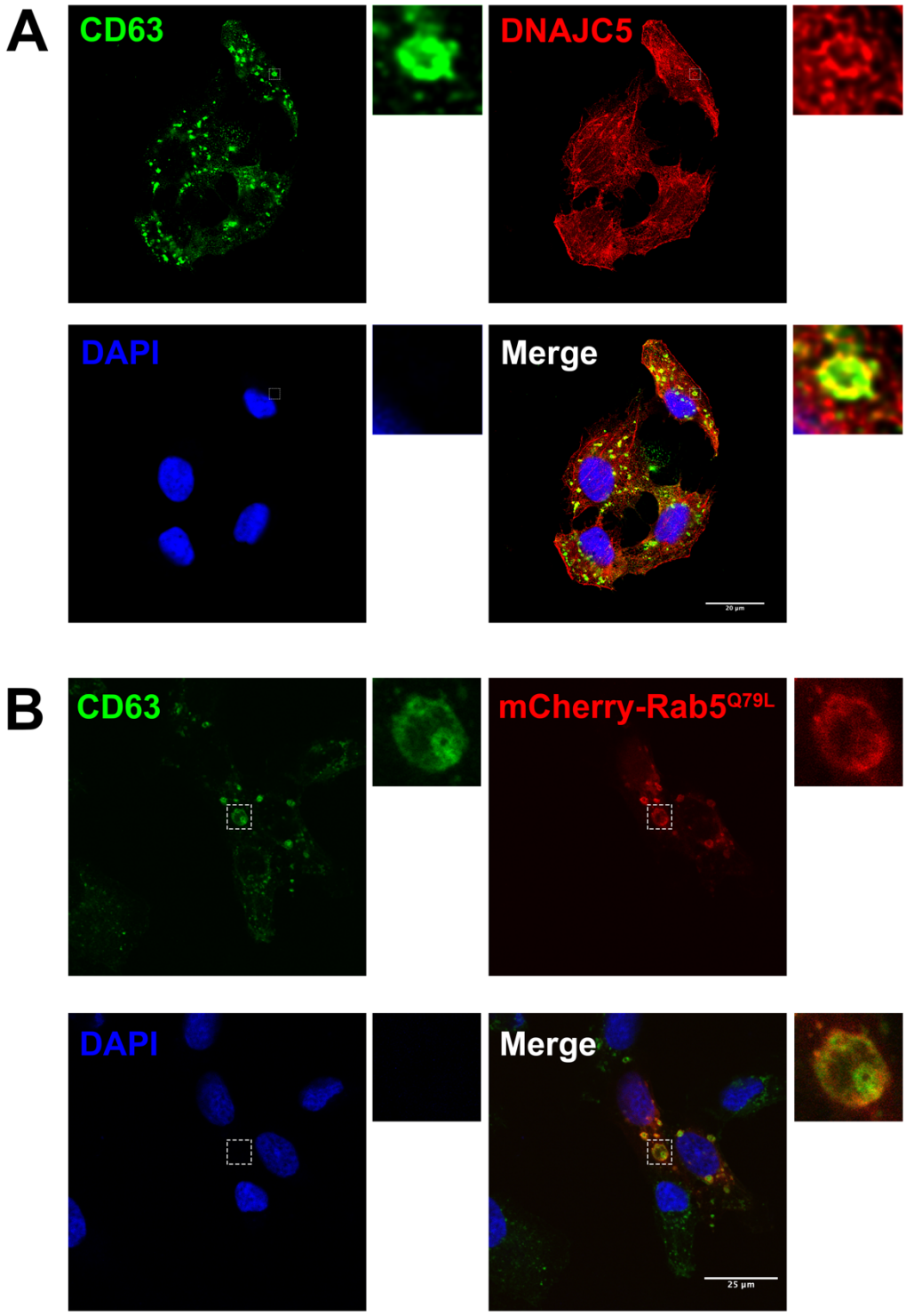

1162

1163 **Figure 4 – figure supplement 2**. Live-cell images of DNAJC5 L115R mutant and

1164 α-syn.

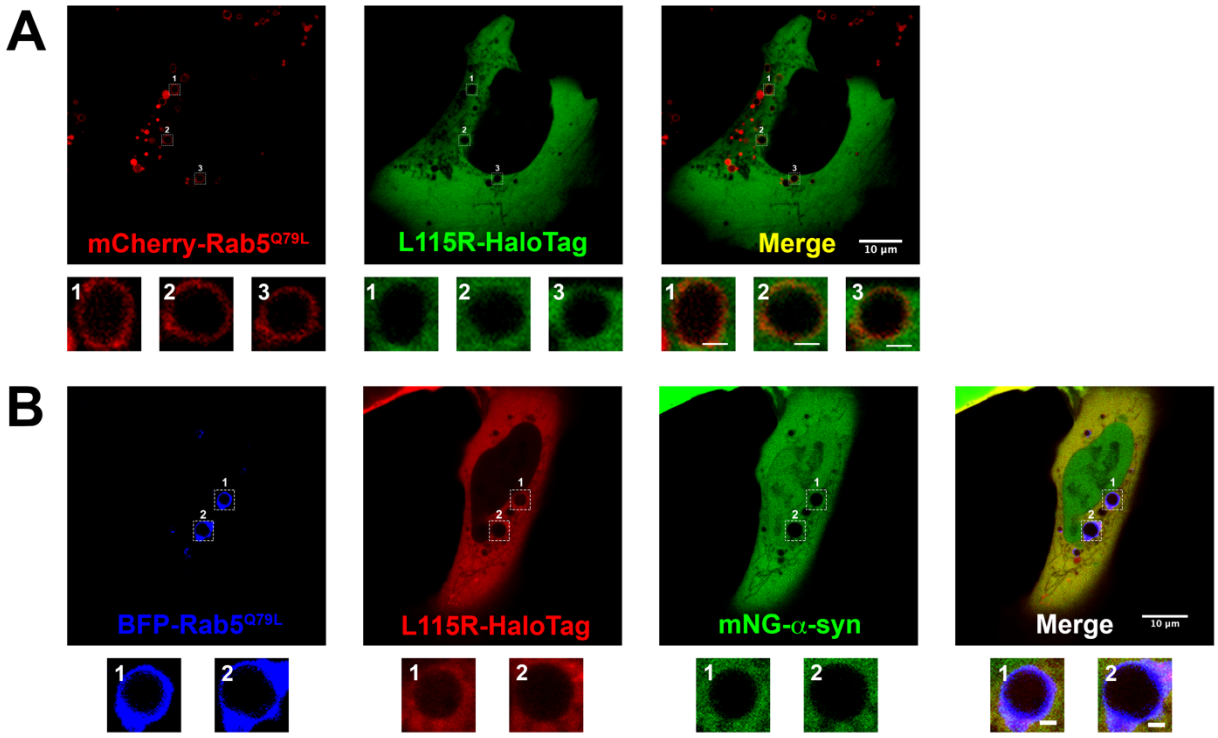

1165

1166

1167 **Figure 4 - supplement video**. Time lapse of movement of internalized α-syn and
1168 DNAJC5 in the enlarged endosomes. Blue, $Rab5^{Q79L}$; Green, α-syn; Red,
1169 DNAJC5. Scale bar: 10 μm.

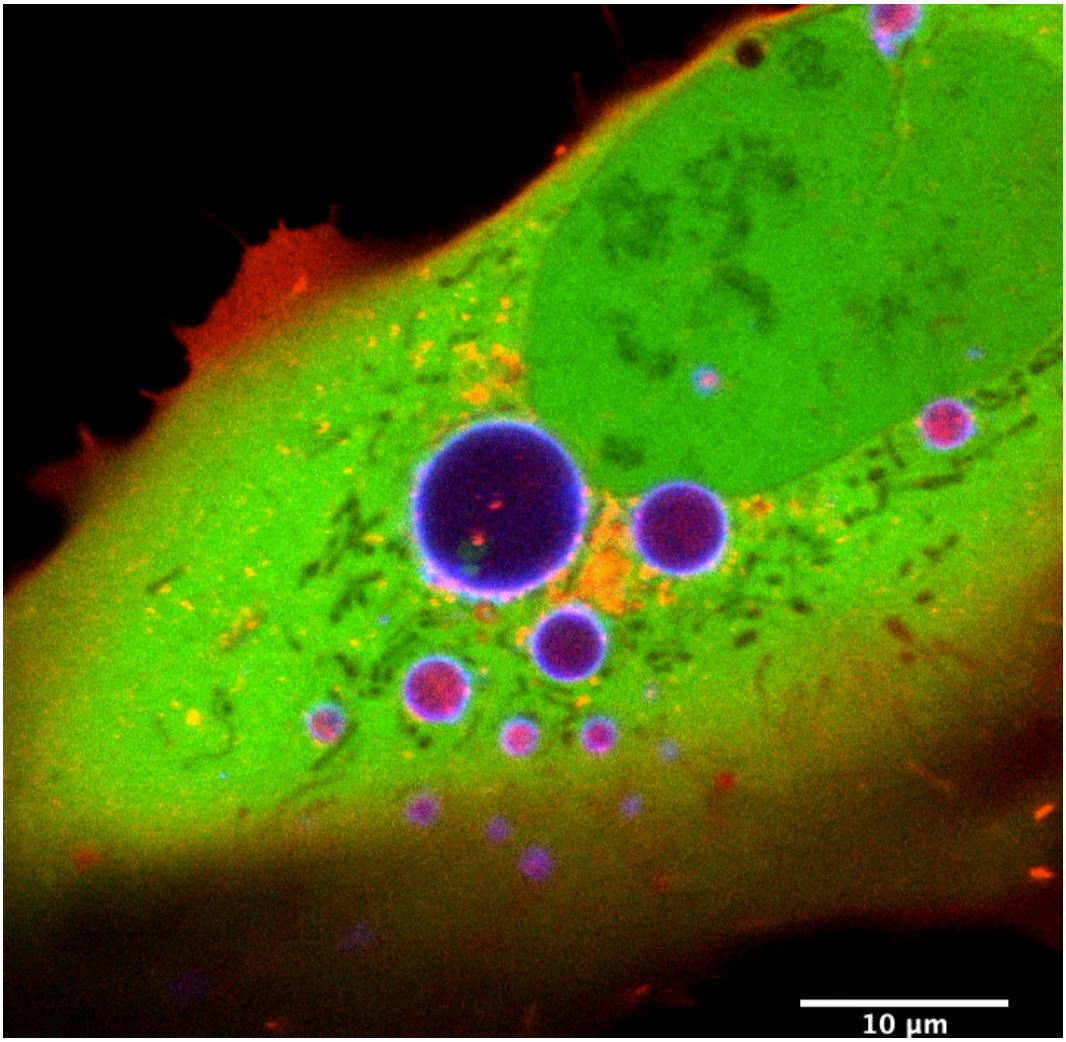

1176

1177 **Figure 5**. Secretion of tandem α-syn oligomers and α-syn fused with thermostable

1178 helix bundles.

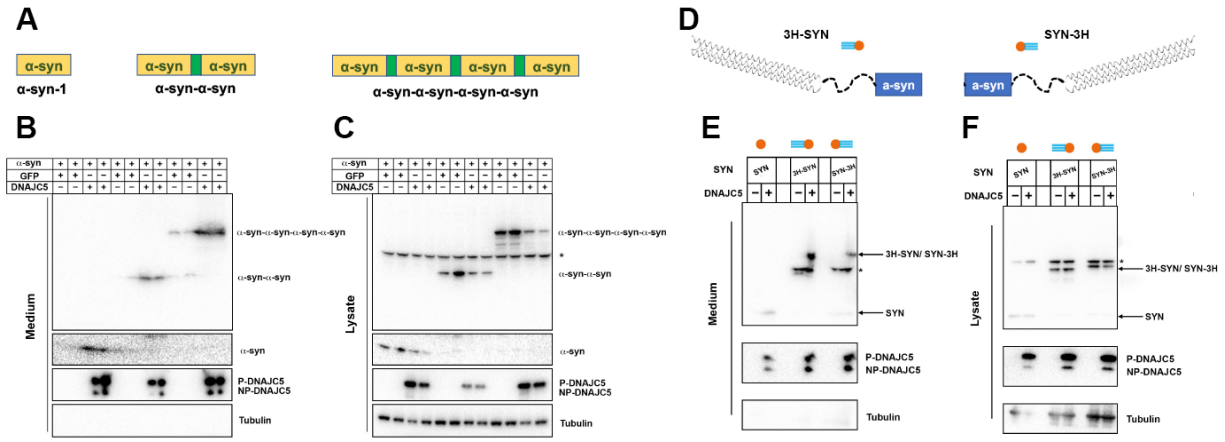

1179

1180

1181 **Figure 5 – figure supplement**. Medium fractionation of secreted tandem α-syn
1182 oligomers. P-DNAJC5 was depleted in the supernatant after centrifugation at
1183 100,000 (100k) xg. However, no significant decrease of tandem α-syn oligomers in
1184 the supernatant was observed.

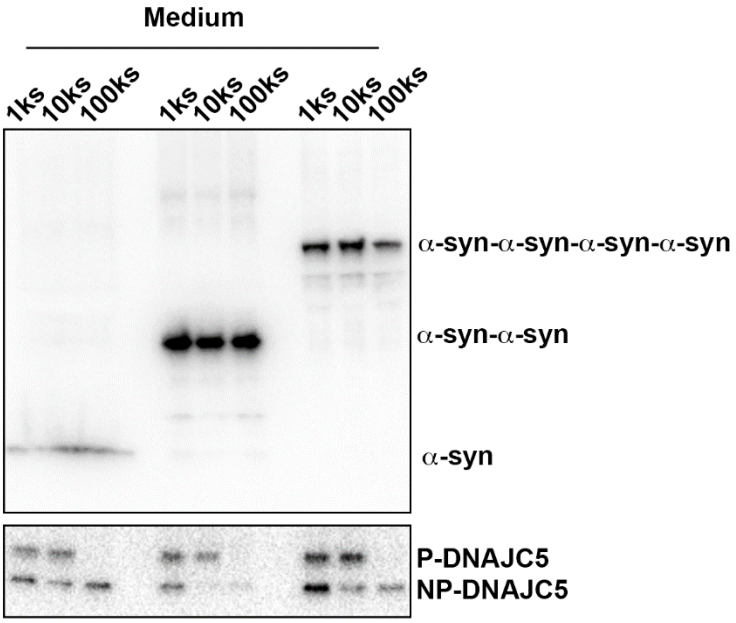

1185

1186

1187 **Figure 6.** XPACK (XP)-induced DNAJC5 L115R oligomerization rescued α-syn

1188 secretion.

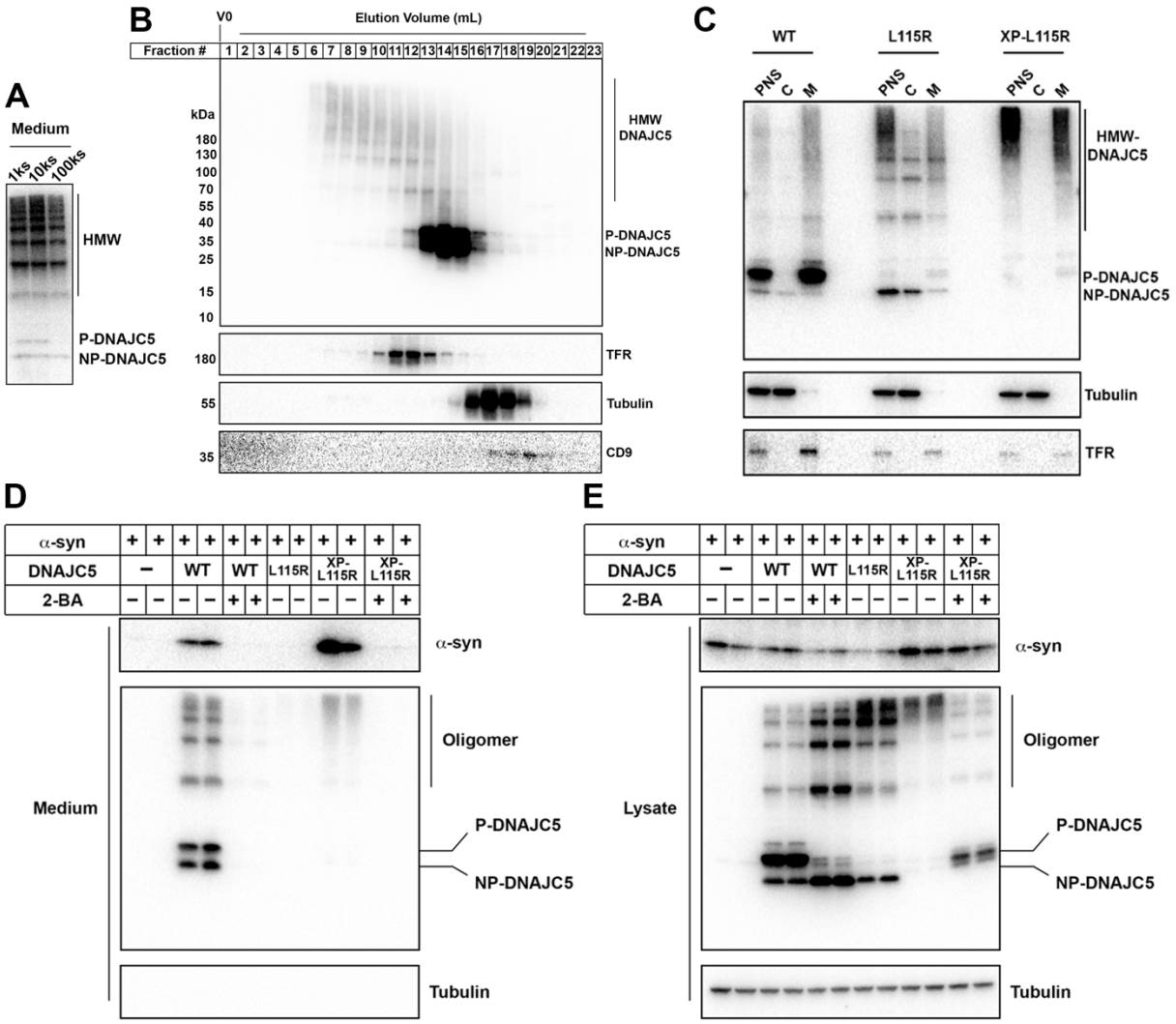

1189

1190

1191 **Figure 6 – figure supplement 1**. Characterization of HMW-DNAJC5 and

1192 XPACK fusion.

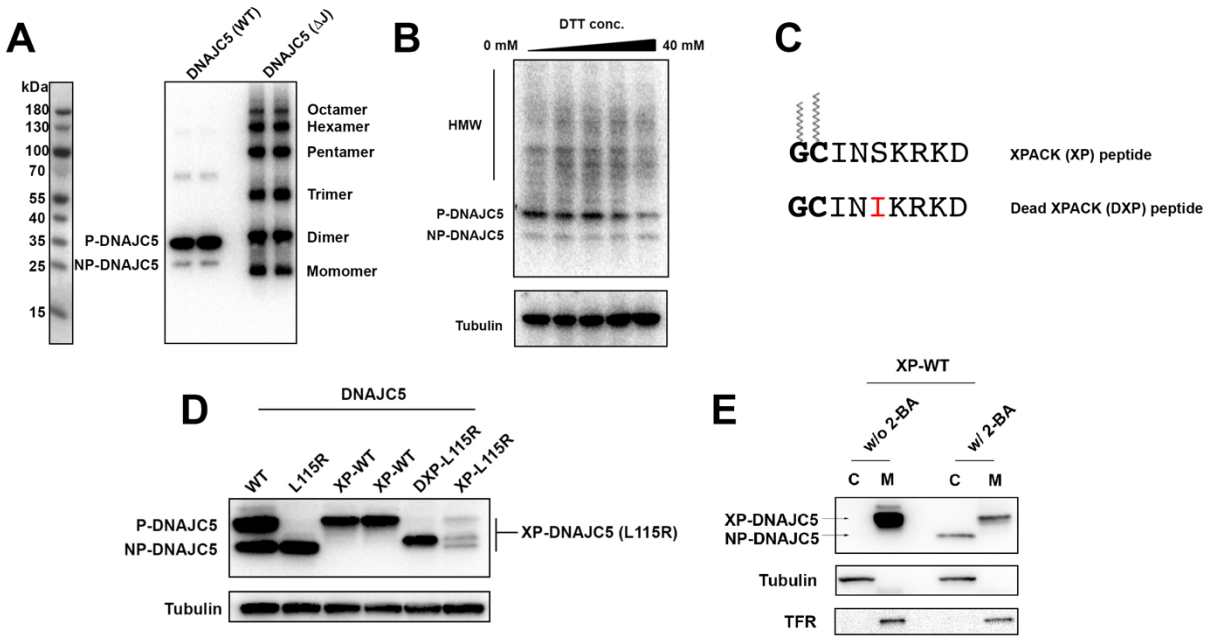

1193

1194

1195 **Figure 6 – figure supplement 2**. Live-cell images of XP-DNAJC5 L115R mutant

1196 and α-syn.

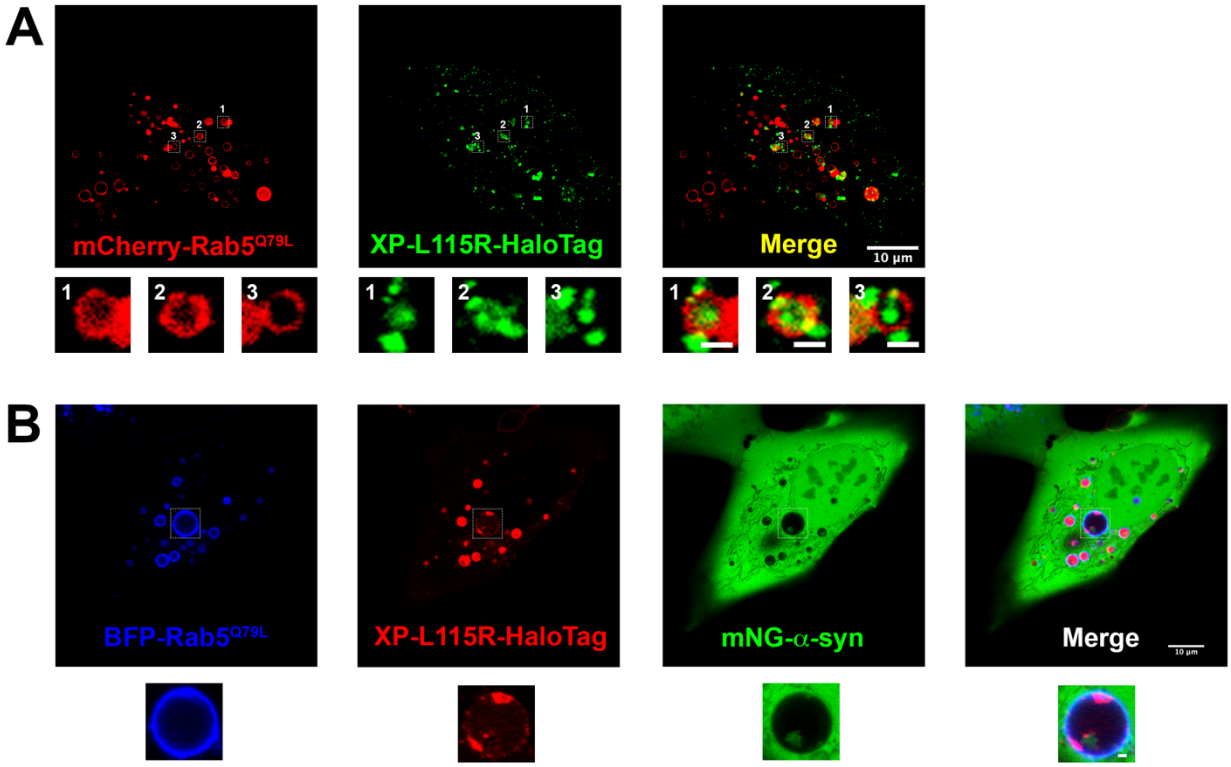

1197

1198

1199 **Figure 7**. Domain mapping of secretion-competent DNAJC5.

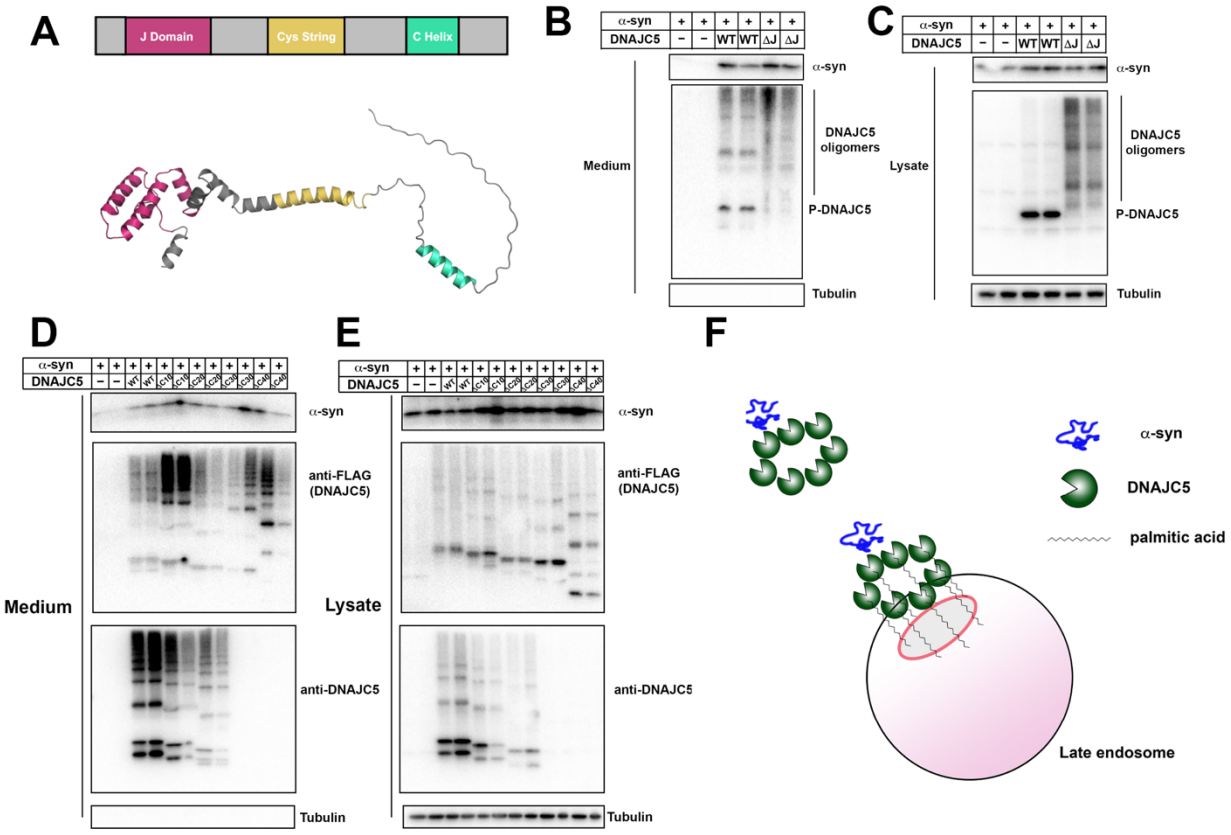

1200

1201

1202

1203